NASA TECHNICAL NOTE

NASA TN D-1998

EFFECTS OF COMPRESSIBILITY AND HEAT TRANSFER ON THE LAMINAR SUBLAYER OF THE TURBULENT BOUNDARY LAYER

by K. R. Czarnecki and William J. Monta

Langley Research Center
Langley Station, Hampton, Va.

NATIONAL AERONAUTICS AND SPACE ADMINISTRATION • WASHINGTON, D. C. • OCTOBER 1964

EFFECTS OF COMPRESSIBILITY AND HEAT TRANSFER ON THE LAMINAR SUBLAYER OF THE TURBULENT BOUNDARY LAYER

By K. R. Czarnecki and William J. Monta

Langley Research Center
Langley Station, Hampton, Va.

NATIONAL AERONAUTICS AND SPACE ADMINISTRATION

For sale by the Office of Technical Services, Department of Commerce,
Washington, D.C. 20230 -- Price $1.25

EFFECTS OF COMPRESSIBILITY AND HEAT TRANSFER ON THE LAMINAR SUBLAYER OF THE TURBULENT BOUNDARY LAYER

By K. R. Czarnecki and William J. Monta
Langley Research Center

SUMMARY

An analytical investigation has been made of the effects of compressibility and heat transfer on the characteristics of the laminar sublayer. The theoretical model consisted of a turbulent boundary layer with a logarithmic nondimensional outer velocity distribution that was not affected by compressibility or heat-transfer effects, and a laminar sublayer that was influenced by these parameters.

The analysis indicates that at zero heat transfer an increase in Mach number at constant free-stream Reynolds number per foot causes an increase in the nondimensional velocities of the sublayer and a rapid increase in the sublayer thickness. This effect is largest where the local skin-friction coefficient is highest. Boundary-layer cooling has a strong effect opposite to that of increasing Mach number. It appears that the laminar sublayer may lie in the slip-flow regime over a wide range of supersonic Mach numbers.

INTRODUCTION

The concept of a laminar sublayer within a turbulent boundary layer has proved to be of great value in explaining certain characteristics of turbulent boundary layers at subsonic speeds. One of these characteristics, which is of great current interest, is concerned with the behavior of the turbulent skin friction when surface roughness is present. For example, the concept has been able to provide a reasonable explanation of the fact that under one set of conditions three-dimensional surface roughness of the sand-grain type had no effect on the turbulent skin friction, whereas, under another set of conditions the roughness would cause a large increase in drag. The explanation (ref. 1, p. 417) was that in the first case the surface roughness was imbedded well within the laminar sublayer where all flow disturbances were damped out. In the second case, the surface roughness protruded beyond the laminar sublayer into a region where vortices were shed from the roughness elements with a resultant increase in drag.

With the development of refined designs for supersonic aircraft in which the proportion of airplane drag assignable to skin friction may be very high,

the problem of predicting the effects of surface roughness takes on added significance. It thus becomes desirable to predict the effects of changes in Mach number on the characteristics of the sublayer. Unfortunately, sufficient reliable experimental data are not available for derivation of trends, and recourse must be made to theory. In this paper some of the trends in laminar sublayer characteristics with changes in Mach number and heat transfer are investigated theoretically; particularly those in the supersonic-speed range.

SYMBOLS

A,B	constants involved in approximation of variation of viscosity of air with temperature by a straight line
a	speed of sound
C	constant of integration
c_p	specific heat of air at constant pressure
d	exponent involved in approximation of variation of viscosity of air with temperature by a power function, and based on wall temperature unless otherwise specified
K	constant involved in approximation of variation of viscosity of air with temperature by a power function
p	static pressure
R	perfect gas constant
R_{ft}	free-stream Reynolds number per foot, $\frac{\rho_\infty u_\infty}{\mu_\infty}$
S	Sutherland gas constant
T	absolute temperature, $^\circ R$
u	velocity parallel to surface
v^*	friction velocity, $\sqrt{\frac{\tau_w}{\rho_w}}$
x	longitudinal distance along surface
y	vertical distance from surface
δ_L	thickness of laminar sublayer

λ mean free path of air

η_r recovery factor, $\frac{T_{aw} - T_\infty}{T_t - T_\infty}$

μ absolute viscosity of air

ν kinematic viscosity of air

ρ mass density of air

τ shear stress

Subscripts:

a viscosity-temperature relationship based on matching Sutherland curve at both free-stream and wall temperatures

aw adiabatic wall

L edge of laminar sublayer

t total or stagnation conditions

w wall

∞ free stream

Dimensionless parameters:

C_f local skin-friction coefficient, $\frac{\tau_w}{\frac{1}{2}\rho_\infty u_\infty^2}$

M Mach number, $\frac{u}{\sqrt{\gamma RT}}$ or $\frac{u}{a}$

R_x Reynolds number based on free-stream conditions and distance x, $\frac{\rho_\infty u_\infty x}{\mu_\infty}$

u^+ velocity parameter, $\frac{u}{v^*}$

y^+ wall distance parameter, $\frac{v^*}{\nu_w} y$

α compressibility parameter, $\frac{\tau_w}{2c_p T_w \rho_w}$

β heat-transfer parameter defined by equation (18)

β' modified heat-transfer parameter defined by equation (A2)

γ ratio of specific heat at constant pressure to specific heat at constant volume

ANALYSIS

Basic Differential Equation

For the purposes of this analysis, the turbulent boundary layer in a compressible flow is assumed to consist of a laminar sublayer and an outer portion with a logarithmic nondimensional velocity distribution. (See fig. 1.) The buffer layer that exists between the two parts of the boundary layer is neglected because there is insufficient information, either theoretical or experimental, to formulate a reliable analysis for this part of the boundary layer in compressible flow. Disregard of the buffer layer will, of course, make the calculation of some finite quantities such as the laminar sublayer thickness somewhat questionable but should not have any significant influence on the trends which are actually the primary concern of this investigation. Additional assumptions are made that the thermal boundary layer is equal in thickness to the velocity boundary layer and that the logarithmic portion of the nondimensional velocity distribution is not affected by changes in Mach number or heat transfer. A study of a large number of supersonic turbulent-boundary-layer profiles indicates the postulate regarding Mach number effect to be a reasonable assumption. (See ref. 2, for example.) For the case of heat transfer, the meager experimental data imply that this assumption probably is not valid. (See ref. 3.) Finally, dissociation effects are neglected and it is assumed that the sublayer is in the continuum-flow regime.

For the flow within the laminar sublayer the viscous shear stress is given by

$$\tau = \mu \frac{du}{dy} \tag{1}$$

This equation is made nondimensional by the use of the following quantities:

$$u^+ \equiv \frac{u}{v^*} \tag{2}$$

$$y^+ \equiv \frac{v^*}{\mu_w/\rho_w} y \tag{3}$$

$$v^* \equiv \sqrt{\frac{\tau_w}{\rho_w}} \tag{4}$$

Substitution of equations (2) to (4) into equation (1) yields

$$\tau = \tau_w \frac{\mu}{\mu_w} \frac{du^+}{dy^+} \tag{5}$$

Because the laminar sublayer is generally very thin, the shear stress τ is assumed to be constant and equal to τ_w, the shear at the wall. Hence,

$$\tau_w = \tau_w \frac{\mu}{\mu_w} \frac{du^+}{dy^+}$$

or

$$dy^+ = \frac{\mu}{\mu_w} du^+ \tag{6}$$

Equation (6) is the basic differential equation which must be solved to obtain the sublayer characteristics.

Conversion of Viscosity Ratio

Viscosity is a function of temperature and can be represented, as will be shown subsequently, by an equation of the form

$$\mu = KT^d \tag{7}$$

where K is some constant and d is an exponent that describes the variation of viscosity of air with temperature. The exponent d is assumed to be a constant for the calculation of the laminar sublayer characteristics at any Mach number or heat-transfer rate, but its value is chosen either on the basis of the temperature at the wall, or on the basis of both the free-stream static temperature and the wall temperature. The value of d thus will vary with Mach number even for the case of zero heat transfer. The viscosity ratio in equation (6) can now be expressed as

$$\frac{\mu}{\mu_w} = \left(\frac{T}{T_w}\right)^d \tag{8}$$

The temperature ratio T/T_w is related to the nondimensional velocity u^+ by means of the quadratic temperature-velocity relation.

$$\frac{T}{T_\infty} = \frac{T_w}{T_\infty} + \frac{T_{aw} - T_w}{T_\infty}\frac{u}{u_\infty} - \frac{T_{aw} - T_\infty}{T_\infty}\left(\frac{u}{u_\infty}\right)^2 \tag{9}$$

Although this temperature-velocity relationship can be strictly applied only to a laminar boundary layer, it should also apply to the first order to the turbulent boundary layer and will certainly be an improvement over the assumption of a Prandtl number of 1 for the purposes of this analysis. A similar approach has been used in reference 4 for the calculation of the turbulent boundary-layer characteristics.

In essence, equation (9) introduces a variable stagnation temperature within the boundary layer. At the wall the stagnation temperature becomes equal to the local wall temperature, which is a function of both the amount of heat transfer involved and the assumed Prandtl number. The Prandtl number effects within the boundary layer are accounted for by a parabolic increase in local stagnation temperature as a function of local velocity, from the adiabatic value at the wall T_{aw} to the free-stream value T_t at the outer edge of the boundary layer. The effects of heat transfer on the stagnation temperature diminish linearly with increase in local velocity from the increment in wall temperature caused by heat transfer $T_{aw} - T_w$ to zero at the edge of the boundary layer.

With the use of the definition of the recovery factor

$$\eta_r \equiv \frac{T_{aw} - T_\infty}{T_t - T_\infty} \tag{10}$$

and of the well-known relationship

$$T_{aw} = T_\infty\left(1 + \eta_r \frac{\gamma - 1}{2} M_\infty^2\right) \tag{11}$$

equation (9) is reduced to

$$\frac{T}{T_\infty} = \frac{T_w}{T_\infty} + \left(1 - \frac{T_w}{T_\infty} + \eta_r \frac{\gamma - 1}{2} M_\infty^2\right)\frac{u}{u_\infty} - \eta_r \frac{\gamma - 1}{2} M_\infty^2\left(\frac{u}{u_\infty}\right)^2 \tag{12}$$

Multiplication of both sides of equation (12) by T_∞/T_w leads to

$$\frac{T}{T_w} = 1 + \left[\frac{T_\infty}{T_w}\left(1 + \eta_r \frac{\gamma - 1}{2} M_\infty^2\right) - 1\right]\frac{u}{u_\infty} - \eta_r \frac{\gamma - 1}{2} M_\infty^2 \frac{T_\infty}{T_w}\left(\frac{u}{u_\infty}\right)^2 \tag{13}$$

With the aid of the defining equations (2) and (4), the definitions

$$M \equiv \frac{u}{a} \tag{14}$$

$$a \equiv \sqrt{\gamma RT} \tag{15}$$

the thermal equation of state

$$\frac{p}{\rho} = RT \tag{16}$$

and the assumption that the static pressure p is constant through the boundary layer, equation (13) is converted to the nondimensional form:

$$\frac{T}{T_w} = 1 + \beta u^+ - \eta_r \alpha u^{+2} \tag{17}$$

where β is defined as the heat-transfer parameter

$$\beta \equiv \sqrt{\frac{\alpha}{\frac{\gamma - 1}{2} M_\infty^2} \frac{T_w}{T_\infty}}\left[\frac{T_\infty}{T_w}\left(1 + \eta_r \frac{\gamma - 1}{2} M_\infty^2\right) - 1\right] \tag{18}$$

and α as the compressibility or friction-heating parameter

$$\alpha = \frac{\tau_w}{2c_p T_w \rho_w} \tag{19}$$

Substitution of equations (8) and (17) into equation (6) results in the nondimensional differential equation

$$dy^+ = \left(1 + \beta u^+ - \eta_r \alpha u^{+2}\right)^d du^+ \tag{20}$$

Conversion of Parameters α and β

The compressibility and heat-transfer parameters α and β can be put into a more convenient form for calculation and for a simpler physical interpretation. The local skin-friction coefficient is defined as

$$C_f \equiv \frac{\tau_w}{\frac{1}{2}\rho_\infty u_\infty^2} \tag{21}$$

Substitution of equation (21) into equation (19) yields with the use of the thermal equation of state (eq. (16)) and the fact that the static pressure through the boundary layer is constant:

$$\alpha = \frac{\frac{C_f}{2} u_\infty^2 \frac{\rho_\infty}{\rho_w}}{2c_p T_w} = \frac{C_f}{2} \frac{1}{2c_p} \frac{u_\infty^2}{T_\infty} \tag{22}$$

From the theorem of conservation of energy

$$c_p T_\infty + \frac{u_\infty^2}{2} = c_p T_t \tag{23}$$

By transposition

$$\frac{u_\infty^2}{T_\infty} = 2c_p\left(\frac{T_t}{T_\infty} - 1\right) \tag{24}$$

Substitution of equation (24) into equation (22) and the fact that

$$\frac{T_t}{T_\infty} = 1 + \frac{\gamma - 1}{2} M_\infty^2 \tag{25}$$

yields

$$\alpha = \frac{C_f}{2} \frac{\gamma - 1}{2} M_\infty^2 = \frac{C_f M_\infty^2}{10} \tag{26}$$

for $\gamma = 1.4$.

The heat-transfer parameter β is converted to a more useful form by substituting equation (26) into equation (18). This substitution yields:

$$\beta = \sqrt{\frac{C_f}{2} \frac{T_w}{T_\infty}}\left[\frac{T_\infty}{T_w}\left(1 + \eta_r \frac{\gamma - 1}{2} M_\infty^2\right) - 1\right] \tag{27}$$

or, if one prefers to use the adiabatic wall temperature directly instead of a recovery factor

$$\beta = \sqrt{\frac{C_f}{2}\frac{T_w}{T_\infty}}\left(\frac{T_{aw}}{T_w} - 1\right) \tag{28}$$

In equations (27) and (28), β is no longer a function of the compressibility or the frictional-heating parameter α; however, β remains dependent upon compressibility effects because of their influence on C_f and T_{aw}.

Sublayer Velocity Distribution

The velocity distributions in question are obtained by the integration of equation (20). This equation cannot be integrated directly for values of d which are of interest inasmuch as d is generally larger than 1/2 but less than 1 (as will be shown subsequently). For integration of equation (20) in its general form for $1/2 < d < 1$, recourse must be made to numerical integration of

$$y^+ = \int_0^{u^+} \left(1 + \beta u^+ - \eta_r \alpha u^{+2}\right)^d du^+ \tag{29}$$

For the case where the heat-transfer parameter β is zero, equation (29) reduces to

$$y^+ = \int_0^{u^+} \left(1 - \eta_r \alpha u^{+2}\right)^d du^+ \tag{30}$$

An expression for the nondimensional velocity distribution within the laminar sublayer can now be obtained for the zero heat-transfer condition from equation (30) by expanding the term

$$\left(1 - \eta_r \alpha u^{+2}\right)^d$$

in a binomial series so that equation (30) becomes

$$dy^+ = \left[1 - \frac{d}{1}\eta_r \alpha u^{+2} + \frac{d(d-1)\eta_r^2 \alpha^2 u^{+4}}{1 \cdot 2} - \frac{d(d-1)(d-2)\eta_r^3 \alpha^3 u^{+6}}{1 \cdot 2 \cdot 3} + \cdots + (-1)^n \frac{d!}{(d-n)!n!}\eta_r^n \alpha^n u^{+2n}\right] du^+ \tag{31}$$

where the series will converge for

$$\left|\eta_r \alpha u^{+2}\right| \leqq 1$$

Integration of this series expression results in

$$y^+ = u^+ - \frac{d\eta_r \alpha u^{+3}}{1 \cdot 3} + \frac{d(d-1)\eta_r^2 \alpha^2 u^{+5}}{1 \cdot 2 \cdot 5} - \frac{d(d-1)(d-2)\eta_r^3 \alpha^3 u^{+7}}{1 \cdot 2 \cdot 3 \cdot 7} + \cdots$$

$$+ (-1)^n \frac{d!}{(d-n)!n!(2n+1)} \eta_r^n \alpha^n u^{+2n+1} \tag{32}$$

$$\left|\eta_r \alpha u^{+2}\right| \leqq 1$$

The use of $u^+ = 0$ when $y^+ = 0$ shows that the constant of integration in equation (32) is zero.

With the elimination of compressibility effects by making $\alpha = 0$ but with the retention of heat-transfer effects equation (29) is converted to

$$y^+ = \int_0^{u^+} (1 + \beta u^+)^d du^+ \tag{33}$$

where β is now given by

$$\beta = \sqrt{\frac{C_f}{2} \frac{T_w}{T_\infty}} \left(\frac{T_\infty}{T_w} - 1 \right) \tag{34}$$

Equation (33) can be integrated for any value of d to give

$$y^+ = \frac{(1 + \beta u^+)^{d+1}}{\beta(d+1)} + C \tag{35}$$

For $y^+ = 0$ and $u^+ = 0$ the constant is found to be

$$C = -\frac{1}{\beta(d+1)}$$

Equation (35) becomes

$$y^+ = \frac{1}{\beta(d+1)}\left[(1+\beta u^+)^{d+1} - 1\right] \tag{36}$$

For α and β both zero, equation (20) reduces to

$$dy^+ = du^+ \tag{37}$$

and equations (32) and (35) reduce to

$$y^+ = u^+ \tag{38}$$

Equations (37) and (38) are the conventional expressions for the nondimensional velocity distributions within the laminar sublayer in incompressible flow with zero heat transfer.

For a Prandtl number of 1 the recovery factor is 1 and the appropriate equations can be simplified accordingly.

Sublayer Thickness

For the calculation of sublayer thicknesses, equation (3) is utilized:

$$\delta_L = y_L = y_L^+ \frac{\mu_w}{\rho_w}\frac{1}{v^*} \tag{39}$$

With the aid of equations (4) and (21), equation (39) is converted to

$$\delta_L = \frac{y_L^+}{R_{ft}\sqrt{\frac{C_f}{2}}}\frac{\mu_w}{\mu_\infty}\sqrt{\frac{T_w}{T_\infty}} \tag{40}$$

With the use of the Sutherland equation

$$\frac{\mu_\infty}{\mu_w} = \left(\frac{T_\infty}{T_w}\right)^{3/2}\left(\frac{T_w + S}{T_\infty + S}\right) \tag{41}$$

where S is the Sutherland constant, equation (40) is converted to

$$\delta_L = \frac{y_L^+}{R_{ft}\sqrt{\frac{C_f}{2}}}\left(\frac{T_w}{T_\infty}\right)^2\left(\frac{1 + \frac{S}{T_\infty}}{\frac{T_w}{T_\infty} + \frac{S}{T_\infty}}\right) \tag{42}$$

where all quantities, exclusive of y_L^+, are known or may be readily calculated from known flight conditions. Sutherland equation is used as a substitute for the viscosity ratio in equation (40) rather than one of the approximate temperature-viscosity relationships, because the corresponding temperature ratios are known exactly and no approximate temperature-viscosity relationships are involved in deriving the equation. Greater accuracy is thus preserved. For incompressible flow and zero heat transfer, equation (42) reduces to the conventional form

$$\delta_L = \frac{y_L^+}{R_{ft}\sqrt{\frac{C_f}{2}}} \tag{43}$$

It should be noted that most of the variables in equation (42) are interrelated and cannot be varied independently of one another. For example, if R_{ft}, T_w/T_∞, and C_f are specified, the value of y_L^+ is fixed. The form of equations (42) and (43) therefore may not necessarily be the most reliable guide as to how a change in any one variable will affect δ_L. Because of the form of the equations for the laminar sublayer and also for the outer-velocity distribution, it is not feasible to obtain explicit analytical expressions for y_L^+ $\left(\text{or } u_L^+\right)$. Values of this parameter must be obtained from plots as will be illustrated subsequently.

Ratio of Sublayer Thickness to Molecular Mean Free Path

From reference 5 the mean free path of a gas is given by

$$\lambda = 1.255\,\frac{\nu}{a}\sqrt{\gamma} \tag{44}$$

and the sublayer thickness as given previously (eq. (39))

$$\delta_L = y_L^+\,\frac{\mu_w}{\rho_w}\,\frac{1}{v^*}$$

The ratio of molecular mean free path to sublayer thickness is

$$\frac{\lambda}{\delta_L} = \frac{1.255 \frac{\nu}{a}\sqrt{\gamma}}{y_L^+ \nu_w \frac{1}{v^*}} \tag{45}$$

If the mean free paths are to be calculated on the basis of conditions at the wall, then

$$\left.\begin{aligned} a &= a_w = \sqrt{\gamma R T_w} \\ \nu &= \nu_w \end{aligned}\right\} \tag{46}$$

Substitution of equations (4), (21), and (46) into equation (45) yields, with the use of

$$M_\infty \equiv \frac{u_\infty}{a_\infty} \tag{47}$$

and the thermal equation of state, the equation

$$\frac{\lambda_w}{\delta_L} = \frac{1.255\sqrt{\gamma} M_\infty \sqrt{\frac{C_f}{2}}}{y_L^+} \tag{48}$$

for the case with or without heat transfer. For a mean free path based on conditions existing at the outer edge of the sublayer, the given values are

$$\left.\begin{aligned} a &= a_L = \sqrt{\gamma R T_L} \\ \nu &= \nu_L \end{aligned}\right\} \tag{49}$$

With the use of the thermal equation of state, the fact that static pressure is constant through the boundary layer and equation (17), the density ratio ρ_L/ρ_w can be expressed as

$$\frac{\rho_L}{\rho_w} = \frac{1}{1 + \beta u_L^+ - \eta_r \alpha u_L^{+2}} \tag{50}$$

Similarly, from equations (8) and (17), the viscosity ratio for the edge of the sublayer becomes

$$\frac{\mu_L}{\mu_w} = \left(1 + \beta u_L^+ - \eta_r \alpha u_L^{+2}\right)^d \tag{51}$$

Substitution of equations (4), (21), (49), (50), and (51) into equation (45) results in

$$\frac{\lambda_L}{\delta_L} = \frac{1.255\left(1 + \beta u_L^+ - \eta_r \alpha u_L^{+2}\right)^{d+1/2} \sqrt{\gamma} M_\infty \sqrt{\frac{C_f}{2}}}{y_L^+} \tag{52}$$

RESULTS AND DISCUSSION

Determination of the Exponent d

For the calculation of the characteristics of the laminar sublayer, it is, of course, desirable to choose the value of the exponent d which provides the best possible representation of the actual variation of viscosity with temperature through the sublayer. The correct variation of viscosity with temperature is given by the Sutherland equation

$$\frac{\mu}{\mu_\infty}\left(\frac{T}{T_\infty}\right)^{3/2}\left(\frac{T_\infty + S}{T + S}\right) \tag{53}$$

where S is the Sutherland constant and is approximately 198.6 for air (ref. 6). The solid-line curves of figure 2 show the values of μ/μ_∞ corresponding to the temperature ratios T/T_∞ encountered within the boundary layer for a Mach number of 3 or 9 with zero heat transfer. The value of T_∞ of 392° R corresponds to the static temperature at an altitude of about 70,000 feet. Included in each of the figures are four approximations to the Sutherland equation. Two of these approximations are of the power form

$$\frac{\mu}{\mu_w} = \left(\frac{T}{T_w}\right)^d$$

given as equation (8) and two are straight-line approximations of the form

$$\frac{\mu}{\mu_w} = A\,\frac{T}{T_w} + B \tag{54}$$

For each type of approximation, the exponents and/or constants were chosen to provide an approximation tangent to the Sutherland curve at the wall temperature ratio (denoted by the subscript w) or to provide an approximation which intersected the Sutherland curve at both wall and free-stream temperature ratios (denoted by the subscript a).

Comparison of the four approximations with the Sutherland curve at both Mach numbers indicates that the best representation of the variation of viscosity with temperature through the laminar sublayer (i.e., the inner portion of the complete turbulent boundary layer) is given by the power form where d is chosen to provide tangency to the Sutherland curve at the wall temperature ratio. This method of determining d is used throughout this paper.

The variation of the value of the exponent d with the Mach number is of interest and is shown in figure 3. The calculations apply to an altitude of 70,000 feet and zero heat transfer. The solid curve is for d determined for tangency to the Sutherland curve at a wall temperature equal to free-stream stagnation temperature. The dashed curve is for d similarly determined, but at an adiabatic wall temperature based on a recovery factor of 0.89.

The curves of figure 3 show that, for the Mach number range investigated, d varies from about 0.84 to 0.53 and decreases as M_∞ increases. The value of d is only slightly affected by changing the wall temperature from a free-stream stagnation temperature to an adiabatic wall temperature based on a recovery factor of 0.89.

Inasmuch as it is desirable to have the best match of the boundary-layer viscosity characteristics near the wall, for the case with heat transfer, d should again be based on the wall temperature. In general, for flights at supersonic speeds a considerable amount of boundary-layer cooling will usually be involved and the value of the exponent d will be higher than that indicated for the zero-heat-transfer case in figure 3, but generally lower than that for the zero-heat-transfer value at $M_\infty = 0$.

Sublayer Velocity Distributions

Some typical changes in the sublayer nondimensional velocity distributions arising from compressibility and heat-transfer effects are presented in figure 4 for Mach numbers of 3, 6, and 9. For the heat-transfer case it was assumed that above $M_\infty = 3$, the surface temperature would be maintained at the level existing at $M_\infty = 3$ without any heat transfer. No calculations were made for the case with boundary-layer heating inasmuch as it is not considered to be a practical condition for even moderate supersonic speeds. Reynolds numbers R_x of 1×10^6, 10×10^6, and 100×10^6 were employed in the calculations. The required values of α and β were obtained with the use of the Sommer and Short T' method for estimating the local skin-friction coefficients (ref. 7). The variation of α over the Mach number range from 0 to 9 for zero heat transfer and for the heat-transfer conditions previously described is shown in figure 5. The logarithmic outer velocity distribution was assumed to be given by (as in ref. 2)

$$u^+ = 5.75 \log y^+ + 5.10 \qquad (55)$$

In all instances, the sublayer curves of figure 4 were obtained by the numerical integration of equation (29), the value of d being chosen to match the appropriate wall temperature. Some additional calculations were made with the use of equation (32) and with the use of an integral form of equation (6) coupled with the Sutherland expression (eq. (41)) for the viscosity ratio. The results of these calculations indicated that the convergence of equation (32) was sufficiently rapid that three terms at moderate or low supersonic Mach numbers, or four terms at higher values would provide results with negligible error compared with those using a larger number of terms. The calculations using equation (32) and the Sutherland distribution for viscosity through the boundary layer indicated an error of considerably less than 2 percent for the most critical case, $M_\infty = 9$, with $R_x = 10^6$. Numerical integration of equation (29) yields results with errors smaller than those quoted for use of equation (32).

For the case with zero heat transfer the curves of figure 4 indicate that the effect of compressibility or of an increasing Mach number is to rotate the curves counterclockwise. Thus, the velocities are shifted to higher values of u^+ at constant y^+ or to lower values of y^+ at constant u^+ as M_∞ increases. This effect is smallest at the lowest Mach number ($M_\infty = 3$) and greatest at the highest Mach number ($M_\infty = 9$); in addition, the effect is least at the highest Reynolds number ($R_x = 100 \times 10^6$) where the local skin-friction coefficients are lowest and greatest at the lowest values ($R_x = 1 \times 10^6$) where the local skin-friction coefficients are highest. In general, the effect of compressibility on the intersection point of the laminar sublayer with the logarithmic outer velocity curve can be significant but not extreme, the maximum change (at $M_\infty = 9$ and $R_x = 1 \times 10^6$) being on the order of 5 percent in u^+ and 9 percent in y^+ from the incompressible-flow case. A check was also made to determine whether the use of a Prandtl number of 1 instead of 0.705 would have any effect. The effects (not shown) on the curves of u^+ as a function of y^+ were to increase slightly the effects of compressibility or Mach number. Most of the effects were derived from the use of the recovery factor in the pertinent equation, practically no effect being derived from the change in d from adiabatic wall temperature to free-stream stagnation temperature.

The effect of boundary-layer cooling to the contrary (figs. 4(b) and 4(c)) was to rotate the sublayer velocity distribution curves in a clockwise direction. Because of the large amount of cooling assumed at $M_\infty = 9$, the greatest changes occurred at this Mach number. At both $M_\infty = 6$ and $M_\infty = 9$, the greatest change also occurred at the lowest Reynolds number and the least at the highest. The assumption that the wall temperature for the heat-transfer case is always equal to the adiabatic wall temperature at $M_\infty = 3$ (for $M_\infty > 3$) insures that the wall temperature at $M_\infty = 6$ and 9 is above the free-stream static temperature. Thus the fact that for these heat-transfer conditions, the sublayer velocity distributions are rotated clockwise relative to the incompressible-flow zero-heat-transfer reference curve shows that within the framework of the present

theory, boundary-layer cooling will have a stronger effect on the sublayer characteristics than an equal amount of frictional heating. This result stems directly from the assumptions of a linear variation of boundary-layer stagnation temperature with velocity for the case of heat transfer and a parabolic variation for the case of the Prandtl number effects. For the worst case considered ($M_\infty = 9$ and $R_x = 10^6$), the increases in u_L^+ and y_L^+ due to cooling were on the order of 15 percent and 90 percent, from the reference value of each at the same Reynolds numbers without cooling, and on the order of 10 percent and 60 percent from the reference value for the incompressible-flow zero-heat-transfer conditions.

A comparison of theory with experiment for the case where the combined effects of compressibility (frictional heating) and boundary-layer heat transfer would have a substantial influence on the sublayer nondimensional velocity distributions was not feasible owing to a lack of reliable experimental data for such conditions. A comparison of theory and experiment data of reference 8 at a Mach number of 9 is made in figure 6 which indicates reasonably good agreement. According to the theory, however, for the basic set of conditions prevailing in the tests under consideration, the effects of boundary-layer cooling approximately cancel the effects of frictional heating. Consequently, the theoretical curve for the velocity distributions varies only slightly from the incompressible zero-heat-transfer curve $u^+ = y^+$. This tendency may be true in a rather broad range of practical operating conditions. An interesting feature to note in the experimental results is that there appears to be only a small buffer layer in the plots of the variation of u^+ with y^+ at $M_\infty = 9$. Because of the shrinking of the complete boundary layer in terms of y^+ as M_∞ is increased, this conclusion may not necessarily extend to the dimensions of the buffer layer in terms of the physical coordinate y.

Sublayer Thickness

The sublayer characteristic of greatest significance to the aerodynamicist is its thickness. Results of some calculations made to investigate the effects of compressibility (frictional heating) and boundary-layer cooling on this thickness δ_L are presented in figures 7 and 8. Figure 7 illustrates the effects of Mach number. For this set of calculations a constant lengthwise station had to be specified (see eq. (42)) in order to make valid comparisons; a length x of 10 feet was chosen. Figure 8 shows the variation of sublayer thickness with surface distance. Required values of y_L^+ for both sets of calculations were obtained from the intersection of the laminar sublayer curves with the outer logarithmic velocity distributions in plots similar to figure 4.

The data of figure 7 indicate that at constant R_{ft} and zero heat transfer, there is a very rapid increase in δ_L with M_∞, the rise from $M_\infty = 0$ to $M_\infty = 9$ being nearly a couple orders of magnitude. Most of this increase in δ_L with M_∞ is due to the large decrease in density in the boundary layer close to the surface and only a minor part is due to the change in sublayer velocity profile and, hence, the change in y_L^+. There is also a large increase in δ_L as

R_{ft} is decreased at constant M_∞; this increase illustrates the strong influence that altitude will have.

The large increases in δ_L indicated for the highest Mach numbers at zero heat transfer cannot be realized in practical situations because of surface cooling requirements. For the case with heat transfer, where for $M_\infty > 3$ the surface temperature is cooled to the adiabatic wall temperature existing at $M_\infty = 3$, the increase in δ_L will be reduced to a factor of about 2 between $M_\infty = 3$ and $M_\infty = 9$. (See dashed lines in fig. 7.) For the heat-transfer case the increment in δ_L due to change in R_{ft} is approximately the same as that for the adiabatic wall case.

For an airplane in flight R_{ft} will not always, or even generally, remain constant as its speed increases. Consequently, some calculations were made for the case where an airplane flies at a constant altitude of 70,000 with R_{ft} variable as M_∞ increases. The same set of zero-heat-transfer and boundary-layer cooling conditions were used as in the constant R_{ft} case. A comparison of these results (short-dashed and dot-dashed curves in fig. 7) with those for constant R_{ft} indicates that the rate of growth of δ_L with M_∞ is curtailed for the constant-altitude case. In fact, for the constant-altitude case with boundary-layer cooling, the sublayer thickness actually decreased with Mach number over part of the range and the overall variation was very small.

The variation in δ_L with surface distance at zero heat transfer (fig. 8(a)) is very small, being approximately a power function with the exponent varying from about 1/12 at the low Mach number and high Reynolds number per foot case to about 1/9 at the high Mach number, low Reynolds number per foot case. For the thinnest sublayer ($M_\infty = 3$, $R_{ft} = 10 \times 10^6$), the increase in δ_L from $x = 1$ foot to $x = 100$ feet is about 40 percent. For the thickest sublayer ($M_\infty = 9$, $R_{ft} = 1 \times 10^6$), the increase over the same distance is still only about 70 percent. The changes in δ_L due to changes in R_{ft} are, of course, very large and again emphasize the strong role that altitude will play in determining sublayer characteristics in actual flight applications. The effect of boundary-layer cooling (fig. 8(b)) is to reduce sharply the sublayer thickness relative to the zero heat-transfer case and to decrease somewhat the variation of δ_L with x.

Relation of Sublayer Thickness to Molecular Mean Free Path

One of the basic assumptions made in this investigation was that the sublayer was in the continuum-flow regime. Inasmuch as some of the sublayers that were calculated are very thin and the density near the surface very low at the higher Mach numbers, some calculations to check the validity of this assumption appear to be desirable. Results of calculations to determine the variation of the ratio λ/δ_L with M_∞ for some of the same conditions for which δ_L was computed in figure 7 are presented in figure 9. Results of calculations to

determine the variation of λ/δ_L with x are presented in figure 10. The latter calculations were limited to the extreme case $M_\infty = 9$ with zero heat transfer. In all instances the calculations were made for the molecular mean free path based on both wall conditions and conditions existing at the outer edge of the sublayer (eqs. (48) and (52)).

The most significant indications of the results presented in figures 9 and 10 are that the ratio λ/δ_L increases with M_∞ both for the case with zero heat transfer (fig. 9(a)) and with boundary-layer cooling (fig. 9(b)) and that there are no unexpected variations of λ/δ_L with x (fig. 10). On the basis that the ratio of molecular mean free path to sublayer thickness is approximately 0.01 for the onset of slip flow, it appears that the laminar sublayer lies in the continuum-flow regime up to a Mach number of 3, but is in the slip-flow regime at Mach numbers greater than $M_\infty = 3$. This conclusion applies whether or not there is any boundary-layer heat transfer.

Effect of Buffer Layer

The present analysis of the laminar sublayer in compressible flow is based on the assumption that there is no buffer layer. In actuality, there is a transitional or buffer region between what might be called the true or viscosity-dominated sublayer and the outer boundary layer of turbulent flow where viscosity plays a minor roll. (See fig. 1.) The true sublayer where viscosity effects predominate and where flow disturbances are strongly damped is thus restricted to a region considerably thinner than the ones calculated in this investigation. It is precisely this thinner inner region of high viscous damping that is of particular interest as regards surface roughness, and, thus, it becomes desirable to speculate as to the effects of including the buffer layer in the analysis of the characteristics of this so-called true laminar sublayer.

First, of course, is the fact that the true laminar sublayer is thinner than the sublayers calculated theoretically. As Mach numbers approach zero, the true sublayer is about one-third or one-fourth of that indicated by theory (ref. 1, p. 405). At higher Mach numbers, particularly for conditions of boundary-layer cooling, this ratio is apparently considerably higher (ref. 8 and fig. 7). In any event, the values of u_L^+ and y_L^+ for the true sublayer will be smaller than those for the theoretical sublayer, and the calculated compressibility and heat-transfer effects are restricted to the inner part of the theoretical sublayer. In this part of the sublayer, the effects on the sublayer nondimensional velocity distributions are smaller than the effects further out. As M_∞ increases, the apparent increase in true sublayer thickness relative to the theoretical value tends to show more of the increased compressibility and heat-transfer effects on the sublayer velocity characteristics calculated for the outer part of the theoretical sublayer. This trend exaggerates the effects of Mach number and tends to compensate for the decrease in Mach number effects resulting from inclusion of the buffer layer.

The true laminar sublayer thickness δ_L will, of course, be smaller than that predicted by a theory which does not include consideration of a buffer

layer. Because δ_L is primarily dependent upon the surface-temperature ratio T_w/T_∞ at constant R_x (y_L^+ in eq. (42) varies only slowly with T_w/T_∞ and M_∞), the relative effects of compressibility and heat transfer on the true sublayer thickness will decrease only slightly with the inclusion of a buffer layer in the analysis. Indeed, the experimental results presented in references 9 and 10 for critical Reynolds number or critical roughness height for which drag due to surface roughness first appears for three-dimensional surface roughness, were analyzed on the basis of the existing wall-temperature ratios, the neglect of compressibility effects on y_L^+, and the omission of the buffer layer; and the analysis was in good agreement with experiment. This result presents a simplified but useful method for approximating the relative effects of Mach number and heat transfer on the true laminar sublayer thickness ratio for practical applications except possibly in the high Mach number range where the increase in $(\delta_L)_{true}$ to $(\delta_L)_{theoretical}$ may increase substantially over the low-speed ratio.

Finally, the fact that the true laminar sublayer is smaller in thickness than the laminar sublayer dealt with in this investigation increases the ratio λ/δ_L and forces the true sublayer further into the slip-flow regime even at the lower supersonic speeds. Thus it may be possible that over most of the supersonic speed range, surface-roughness effects may be dependent more upon slip-flow effects than upon viscous damping.

CONCLUSIONS

An analytical investigation has been made of the effects of compressibility and heat transfer on the characteristics of the laminar sublayer. The theoretical model consisted of a turbulent boundary layer with a logarithmic nondimensional outer velocity distribution that was not affected by compressibility or heat-transfer effects and a laminar sublayer that was influenced by these parameters.

The analysis indicates that at zero heat transfer an increase in Mach number causes an increase in sublayer nondimensional velocities and a rapid increase in sublayer thickness. This effect is largest where the local skin-friction coefficient is highest, whether from nearness to the origin of the turbulent boundary layer or from low free-stream Reynolds number per foot. Boundary-layer cooling has a strong effect opposite to that of increasing Mach number. It appears that the laminar sublayer may lie in the slip-flow regime for a wide range of supersonic Mach numbers.

Langley Research Center,
National Aeronautics and Space Administration,
Langley Station, Hampton, Va., August 4, 1964.

APPENDIX

CHARTS FOR ESTIMATION OF LAMINAR SUBLAYER THICKNESS

If both sides of the laminar sublayer equation (29) are multiplied by $\sqrt{\alpha}$ and if it is noted that the definition of β in equation (18) already incorporates this term, the ensuing equation can be written as

$$y^+\sqrt{\alpha} = \int_0^{u^+\sqrt{\alpha}} \left[1 + \beta' u^+\sqrt{\alpha} - \eta_r\left(u^+\sqrt{\alpha}\right)^2\right]^d d\left(u^+\sqrt{\alpha}\right) \tag{A1}$$

where the modified heat-transfer parameter β' is defined as

$$\beta' \equiv \frac{\beta}{\sqrt{\alpha}} = \sqrt{\frac{1}{\frac{\gamma - 1}{2} M_\infty^2} \frac{T_w}{T_\infty}} \left[\frac{T_w}{T_\infty}\left(1 + \eta_r \frac{\gamma - 1}{2} M_\infty^2\right) - 1\right] \tag{A2}$$

Now it is possible to make charts of $y^+\sqrt{\alpha}$ as a function of $u^+\sqrt{\alpha}$ with the modified heat-transfer parameter β' and the viscosity exponent d as parameters.

In order to simplify the calculation of the laminar sublayer thickness $\delta_L = f\left(y_L^+\right)$, it is necessary to transform the expression for the logarithmic outer part of the turbulent boundary layer (eq. (55)) to the same basic variables and present these curves on the same charts. Multiplication of both sides of equation (55) by $\sqrt{\alpha}$ and conversion of y^+ to $y^+\sqrt{\alpha}$ yields

$$u^+\sqrt{\alpha} = 5.75\sqrt{\alpha}\left(\log y^+\sqrt{\alpha} - \log\sqrt{\alpha}\right) + 5.10\sqrt{\alpha} \tag{A3}$$

In terms of the variables $u^+\sqrt{\alpha}$ and $y^+\sqrt{\alpha}$, this equation must be plotted with $\sqrt{\alpha}$ as a parameter.

Finally, it is desirable to establish a simple relation for the determination of the exponent d in terms of wall temperature. This result is achieved by the logarithmic differentiation of the Sutherland equation expressed in the form

$$\mu = \frac{2.270 \times 10^{-8} T_w^{3/2}}{T_w + S} \tag{A4}$$

with respect to the wall temperature T_w to yield

$$d = \frac{d(\log \mu)}{d(\log T_w)} = \frac{3}{2} - \frac{T_w}{T_w + S} \tag{A5}$$

where S, the Sutherland constant, is taken as approximately 198.6 for air.

Estimation charts based on the laminar sublayer and the outer logarithmic velocity-distribution equations (eqs. (A1) and (A3)) are presented in figure 11. In the figure $u^+\sqrt{\alpha}$ is plotted as a function of $y^+\sqrt{\alpha}$ with β' as the parameter for the sublayer curves, $\sqrt{\alpha}$ as the parameter for the outer logarithmic portion of the boundary layer, with d held constant. Each part of the figure is for a different value of d. The range in β' is from 0 to 2.5 in increments of 0.5 and covers most of the boundary-layer cooling conditions that might actually be experienced. No calculations were made for the boundary-layer-heating cases. The range for d was from 0.5 to 0.9 in increments of 0.1 and again covers most of the conditions that will be actually encountered in flight. The value of d for the known flight conditions can readily be established from figure 13, which is based on equation (A5).

In order to utilize the charts, it is first necessary to determine $\sqrt{\alpha}$ by the use of equation (26), where C_f is determined by some appropriate theory for the flight conditions of interest. Next the value of the modified heat-transfer parameter β' must be established with the aid of equation (A2). With the use of these parameters, it is possible to interpolate the corresponding values of $u_L^+\sqrt{\alpha}$ and $y_L^+\sqrt{\alpha}$ on the charts for each value of d above and below the flight value of d established in figure 12. A linear interpolation of these values to the flight value of d will usually suffice. For greater accuracy the values of $u_L^+\sqrt{\alpha}$ and $y_L^+\sqrt{\alpha}$ can be interpolated over the full range of d and a plot made and faired from which the flight values can be established very accurately.

If a plot of the sublayer nondimensional velocity distribution is desired, a curve must be passed through $u_L^+\sqrt{\alpha}$ and $y_L^+\sqrt{\alpha}$ on each chart parallel to the neighboring β' = constant curves. A set of $u_L^+\sqrt{\alpha}$ values ranging over the complete laminar sublayer is chosen and the corresponding $y^+\sqrt{\alpha}$ values are determined from this curve. These $u^+\sqrt{\alpha}$ and $y^+\sqrt{\alpha}$ values are corrected for the proper flight value of d just as the values of $u_L^+\sqrt{\alpha}$ and $y_L^+\sqrt{\alpha}$ were. Division of $u^+\sqrt{\alpha}$ and $y^+\sqrt{\alpha}$ by $\sqrt{\alpha}$ will provide the desired parameters u^+ and y^+.

REFERENCES

1. Schlichting, Hermann (J. Kestin, trans.): Boundary Layer Theory. McGraw-Hill Book Co., Inc., 1955.

2. Matting, Fred W., Chapman, Dean R., Nyholm, Jack R., and Thomas, Andrew G.: Turbulent Skin Friction at High Mach Numbers and Reynolds Numbers in Air and Helium. NASA TR R-82, 1961.

3. Lobb, R. Kenneth, Winkler, Eva M., and Persh, Jerome: Experimental Investigation of Turbulent Boundary Layers in Hypersonic Flow. Jour. Aero. Sci., vol. 22, no. 1, Jan. 1955, pp. 1-9, 50.

4. Persh, Jerome: A Theoretical Investigation of the Effect of Injection of Air on Turbulent Boundary-Layer Skin-Friction and Heat-Transfer Coefficients at Supersonic and Hypersonic Speeds. NAVORD Rep. 4220, U.S. Naval Ord. Lab. (White Oak, Md.), Jan. 4, 1957.

5. Truitt, Robert Wesley: Fundamentals of Aerodynamic Heating. The Ronald Press Co., c.1960.

6. Ames Research Staff: Equations, Tables, and Charts for Compressible Flow. NACA Rep. 1135, 1953. (Supersedes NACA TN 1428.)

7. Sommer, Simon C., and Short, Barbara J.: Free-Flight Measurements of Turbulent-Boundary-Layer Skin Friction in the Presence of Severe Aerodynamic Heating at Mach Numbers From 2.8 to 7.0. NACA TN 3391, 1955.

8. Hill, F. K.: Boundary-Layer Measurements in Hypersonic Flow. Jour. Aero. Sci., vol. 23, no. 1, Jan. 1956, pp. 35-42.

9. Sevier, John R., Jr., and Czarnecki, K. R.: Investigation of Effects of Distributed Surface Roughness on a Turbulent Boundary Layer Over a Body of Revolution at a Mach Number of 2.01. NACA TN 4183, 1958.

10. Czarnecki, K. R., Sevier, John R., Jr., and Carmel, Melvin M.: Effects of Fabrication-Type Roughness on Turbulent Skin Friction at Supersonic Speeds. NACA TN 4299, 1958.

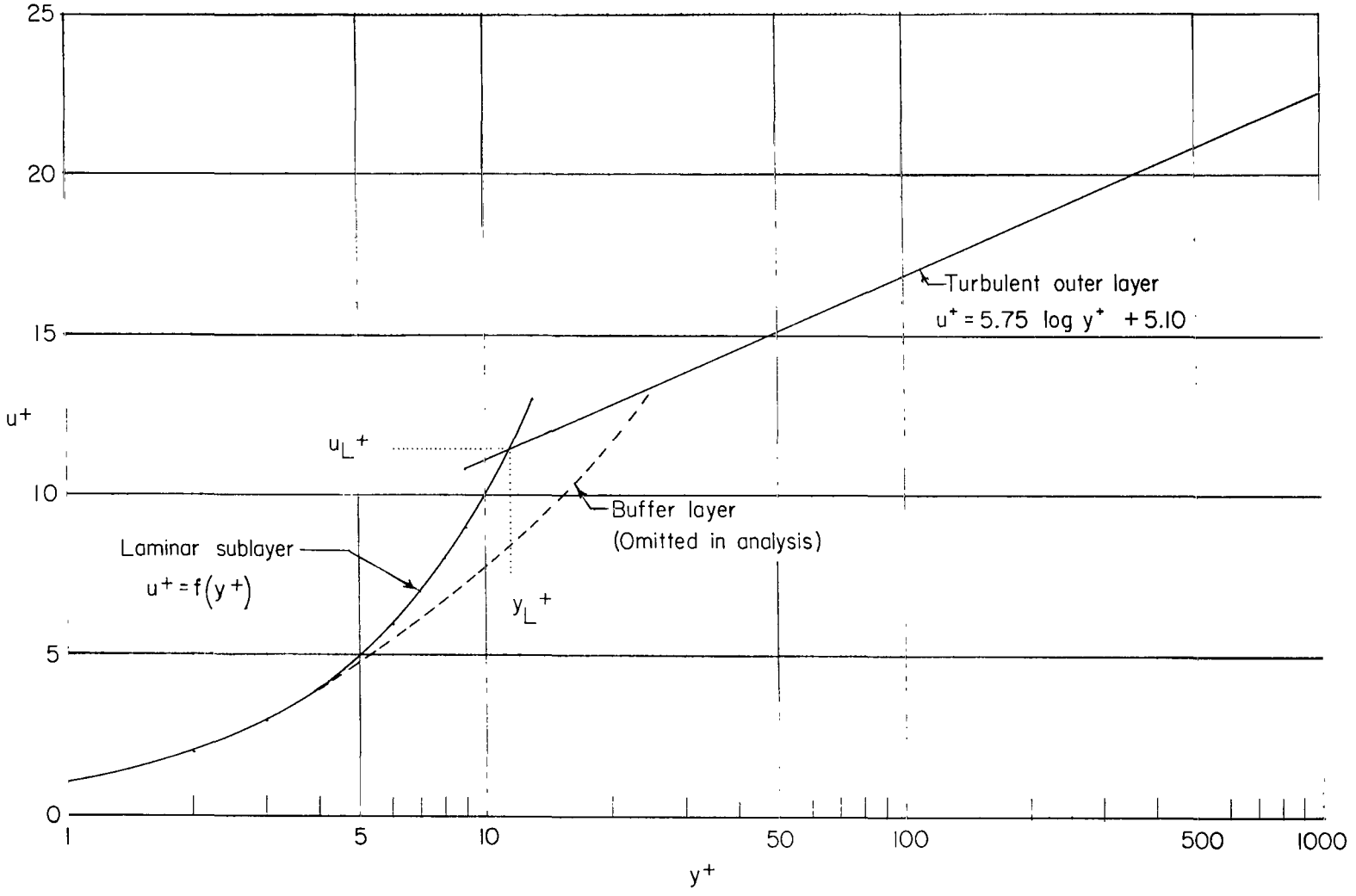

Figure 1.- Assumed model of laminar sublayer in a compressible turbulent boundary layer.

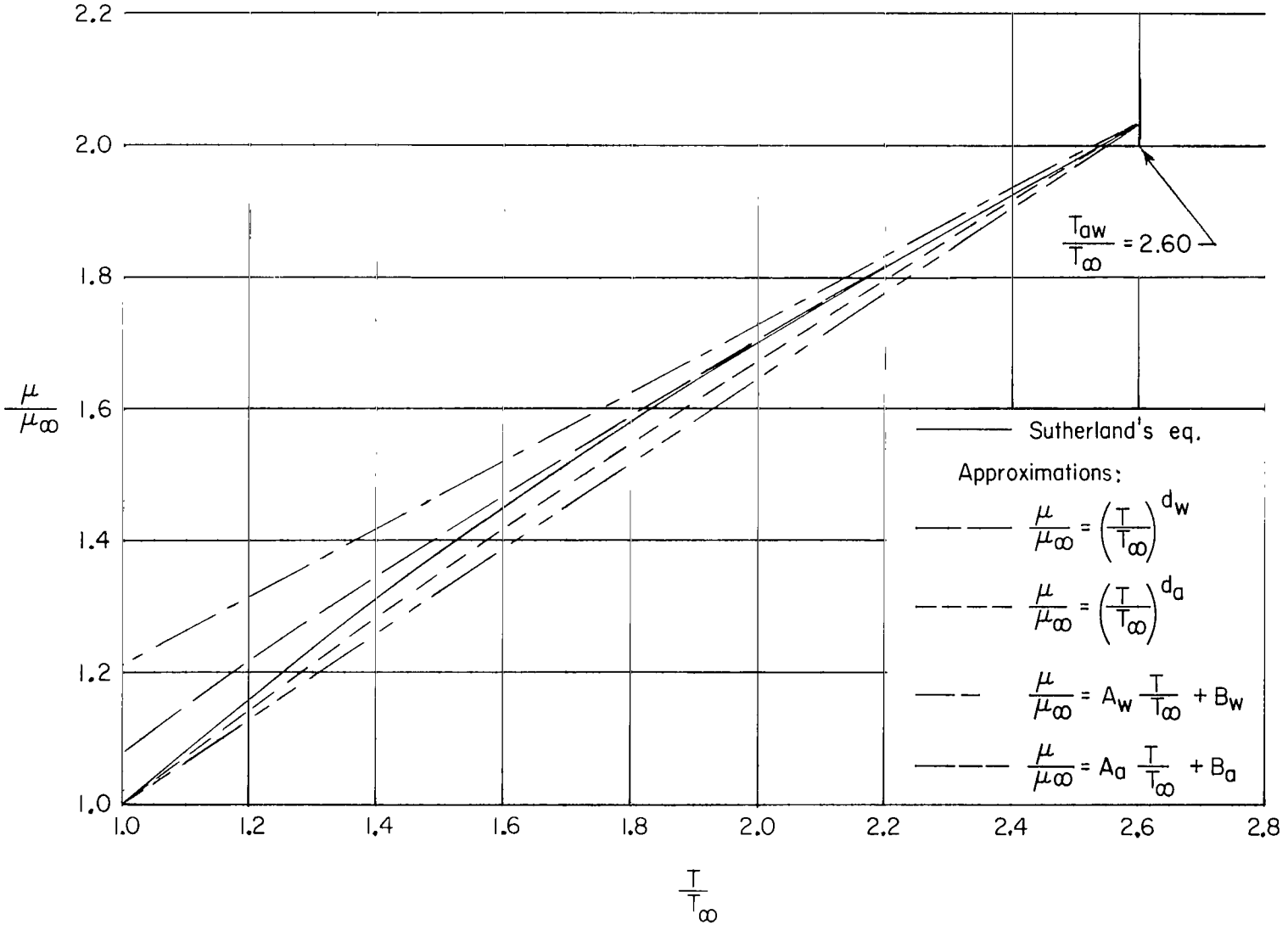

(a) $M_\infty = 3$.

Figure 2.- Variation of viscosity ratio with temperature ratio shown by Sutherland's equation and several approximations. Zero heat transfer; $T_\infty = 392^\circ$ R.

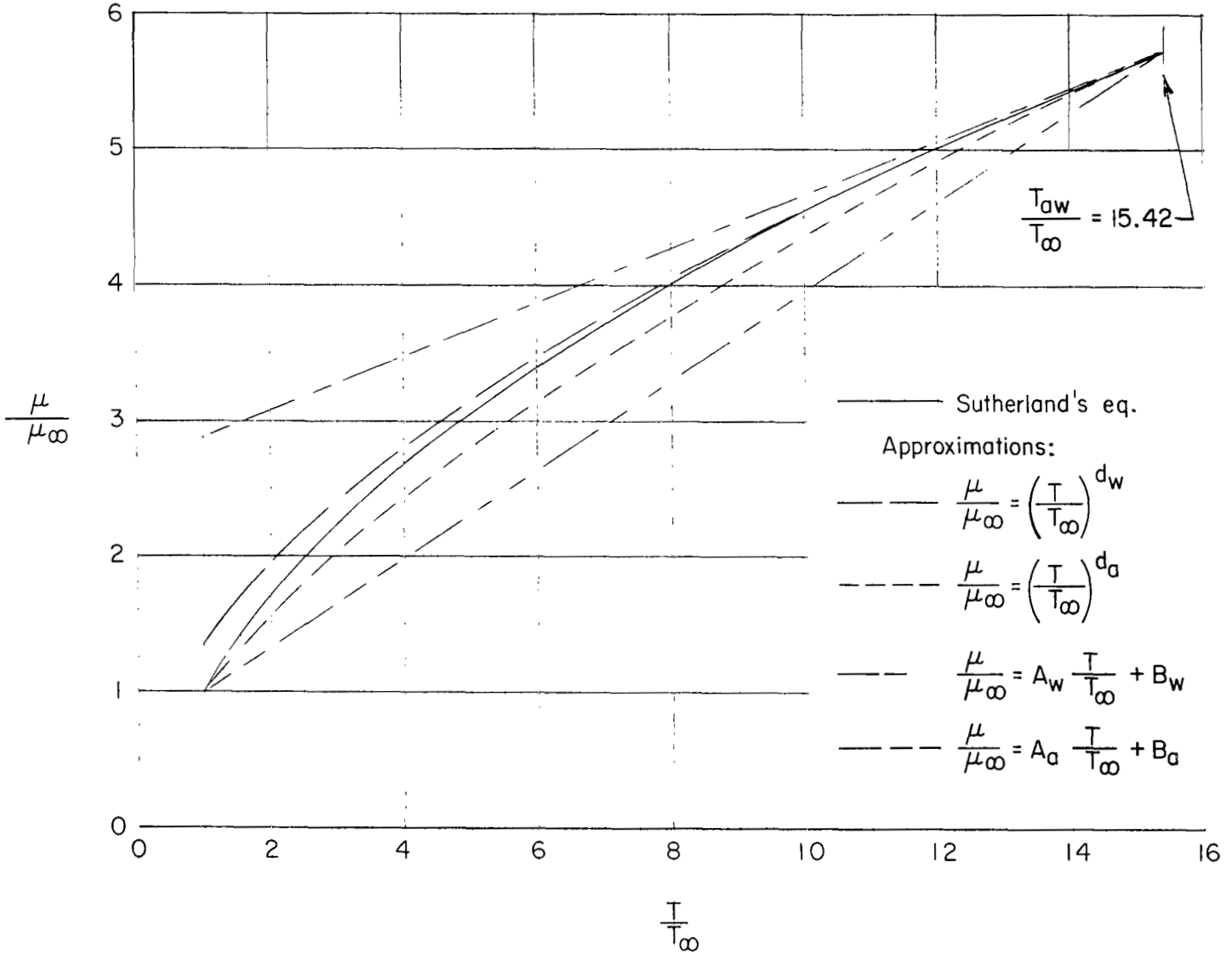

(b) $M_\infty = 9$.

Figure 2.- Concluded.

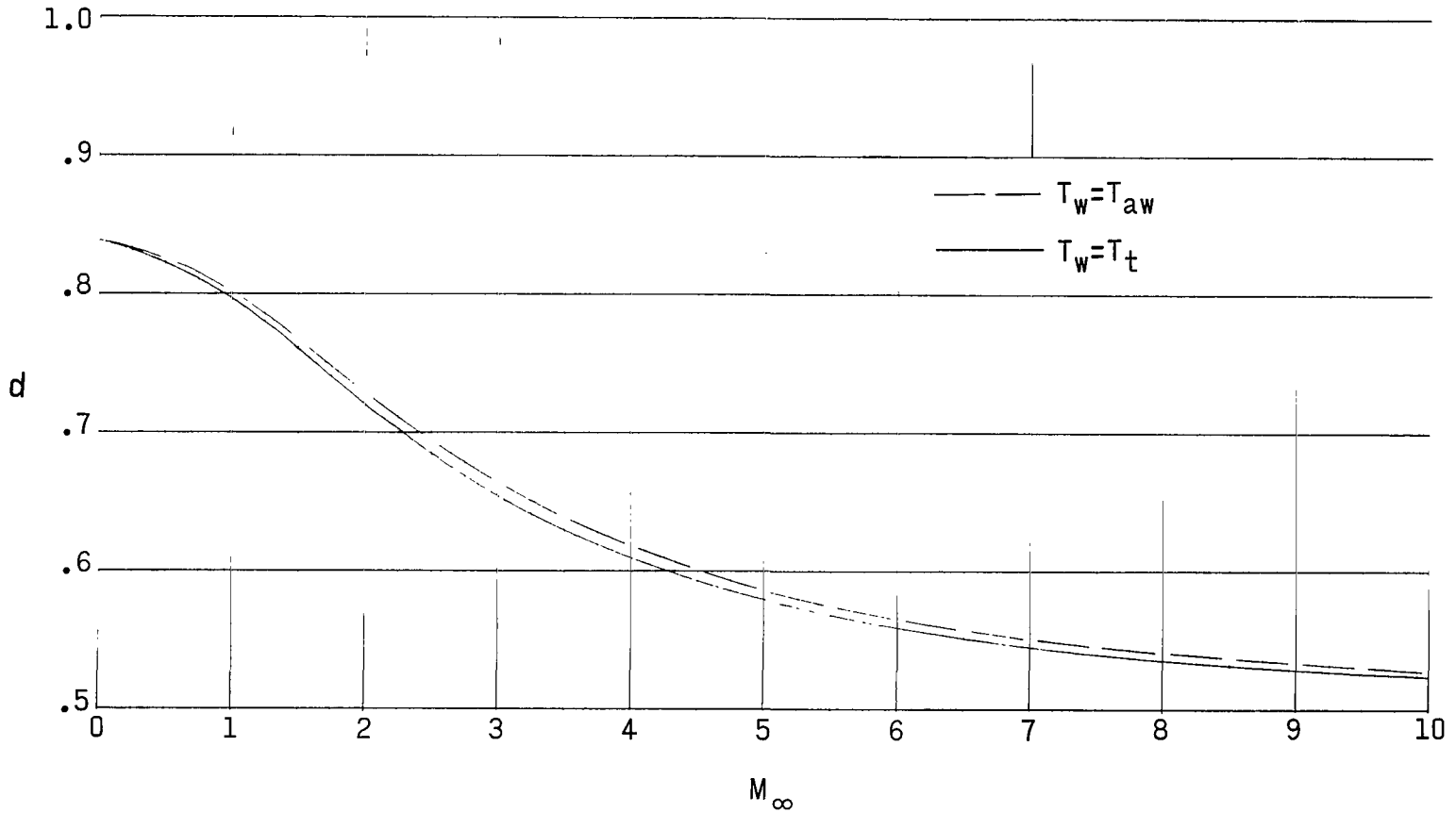

Figure 3.- Variation of the viscosity-law exponent d with M_∞. Zero heat transfer; $T_\infty = 392^\circ$ R.

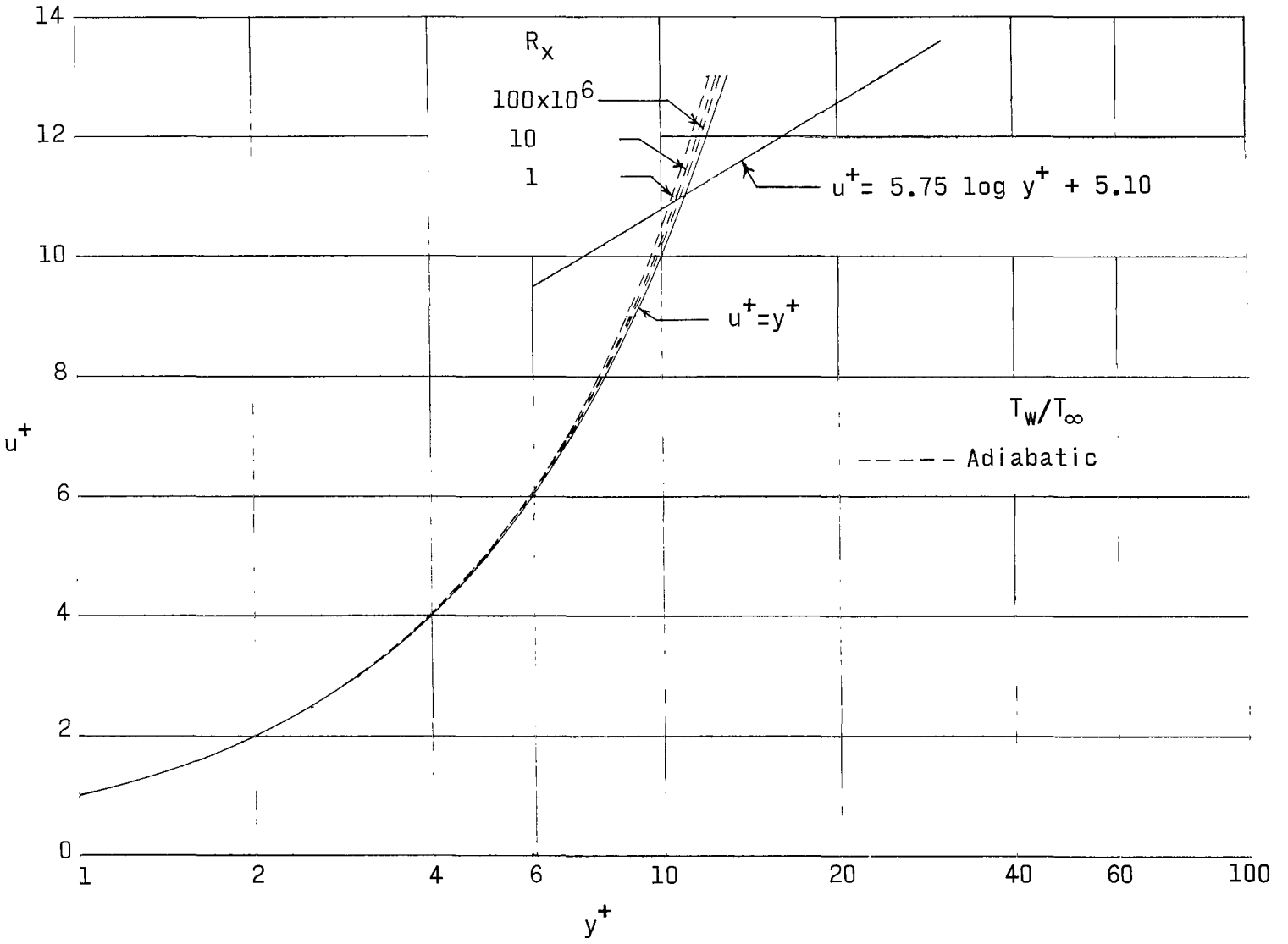

(a) $M_\infty = 3$.

Figure 4.- Variation in laminar sublayer nondimensional velocity profile with R_x. $T_\infty = 392^\circ$ R.

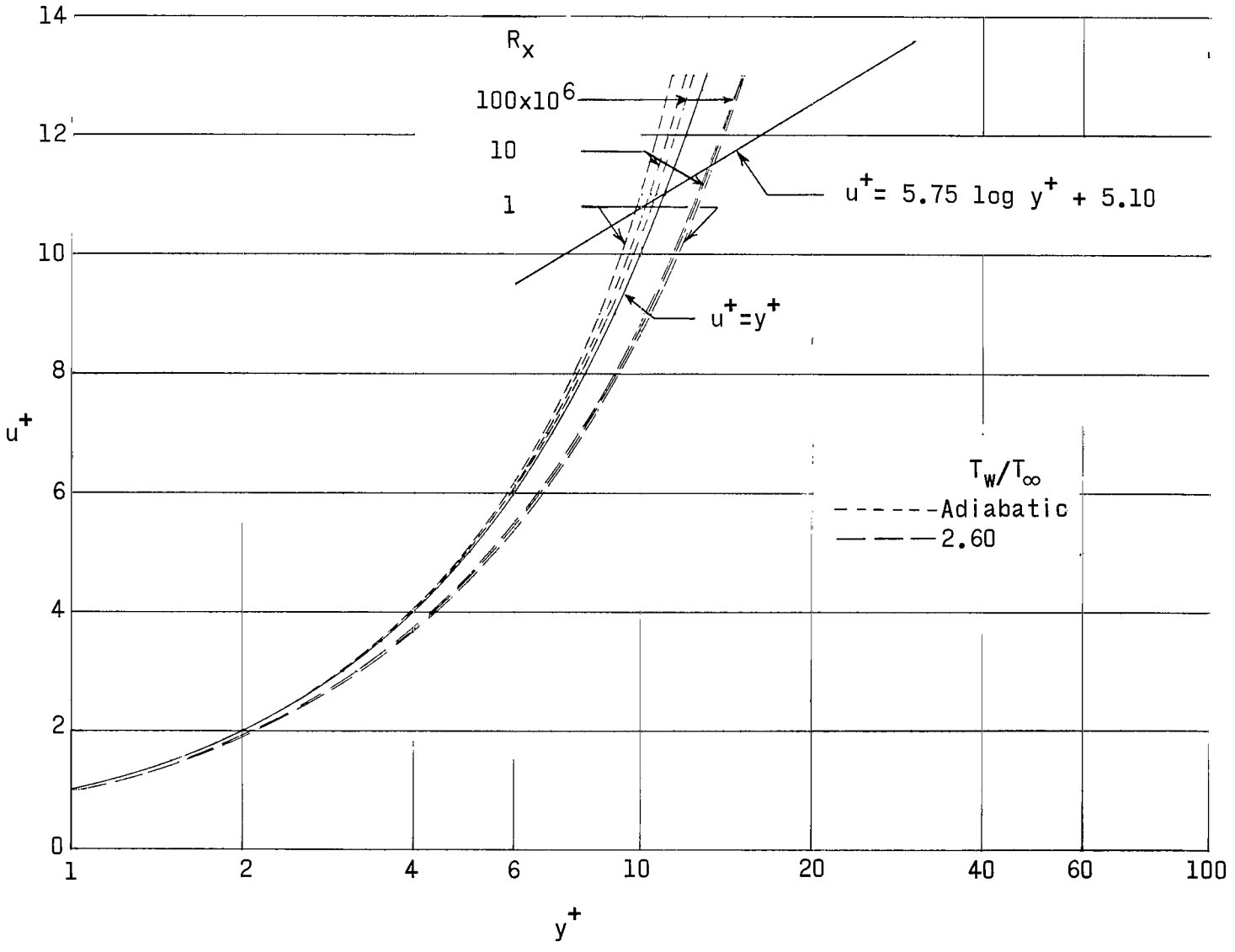

(b) $M_\infty = 6$.

Figure 4.- Continued.

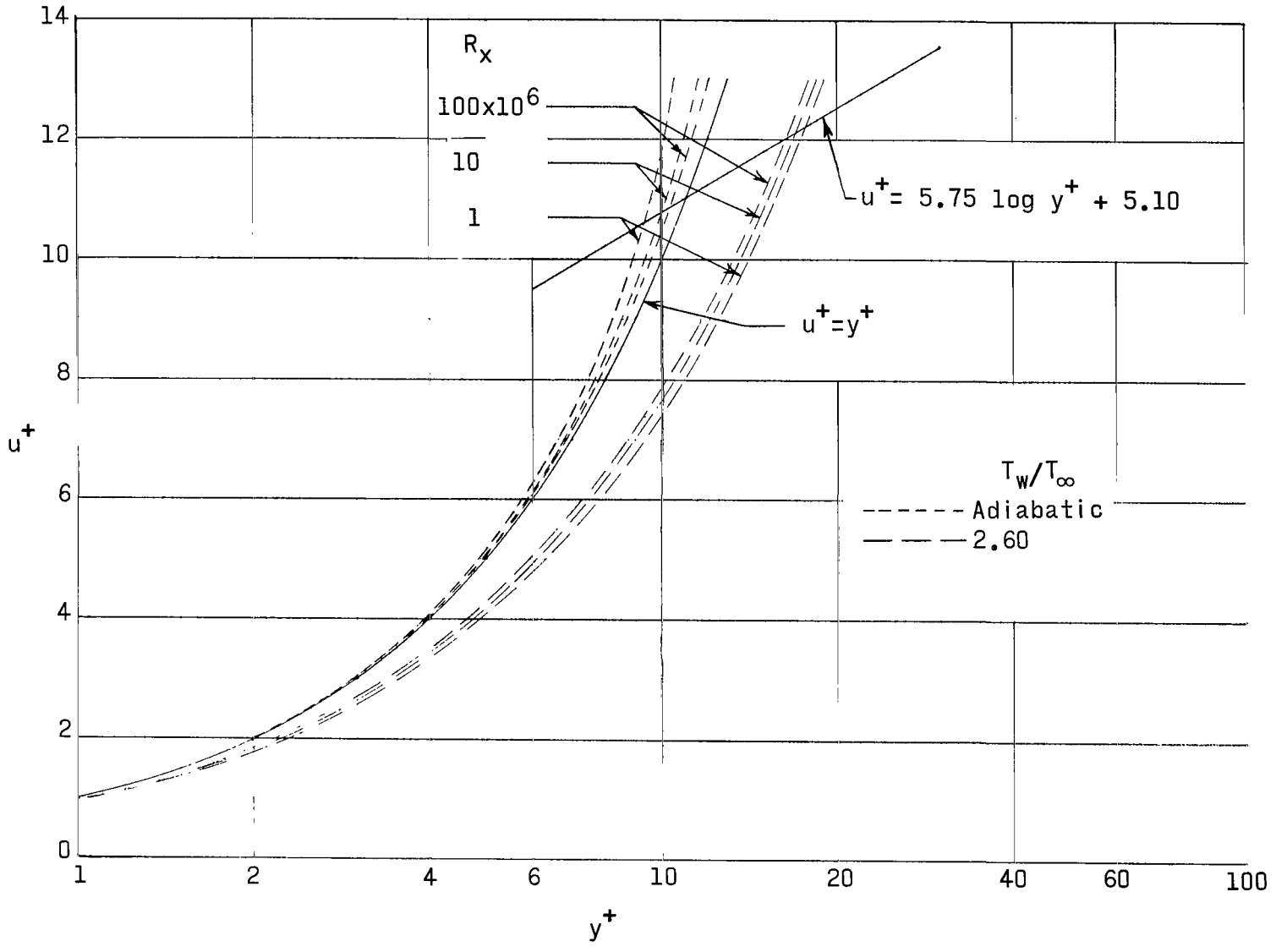

(c) $M_\infty = 9$.

Figure 4.- Concluded.

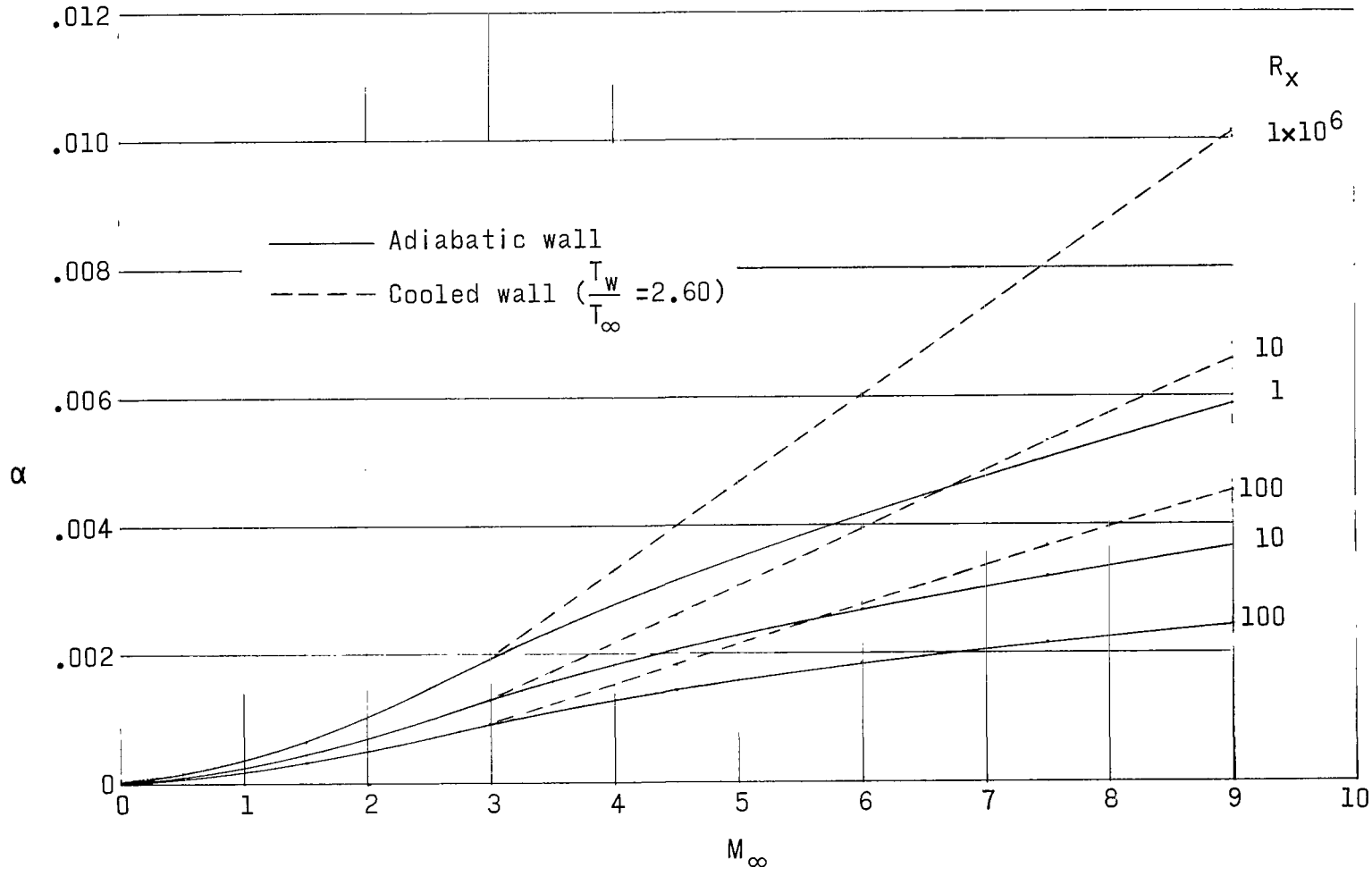

Figure 5.- Variation of α with M_∞ for various values of R_x; $T_\infty = 392^\circ$ R.

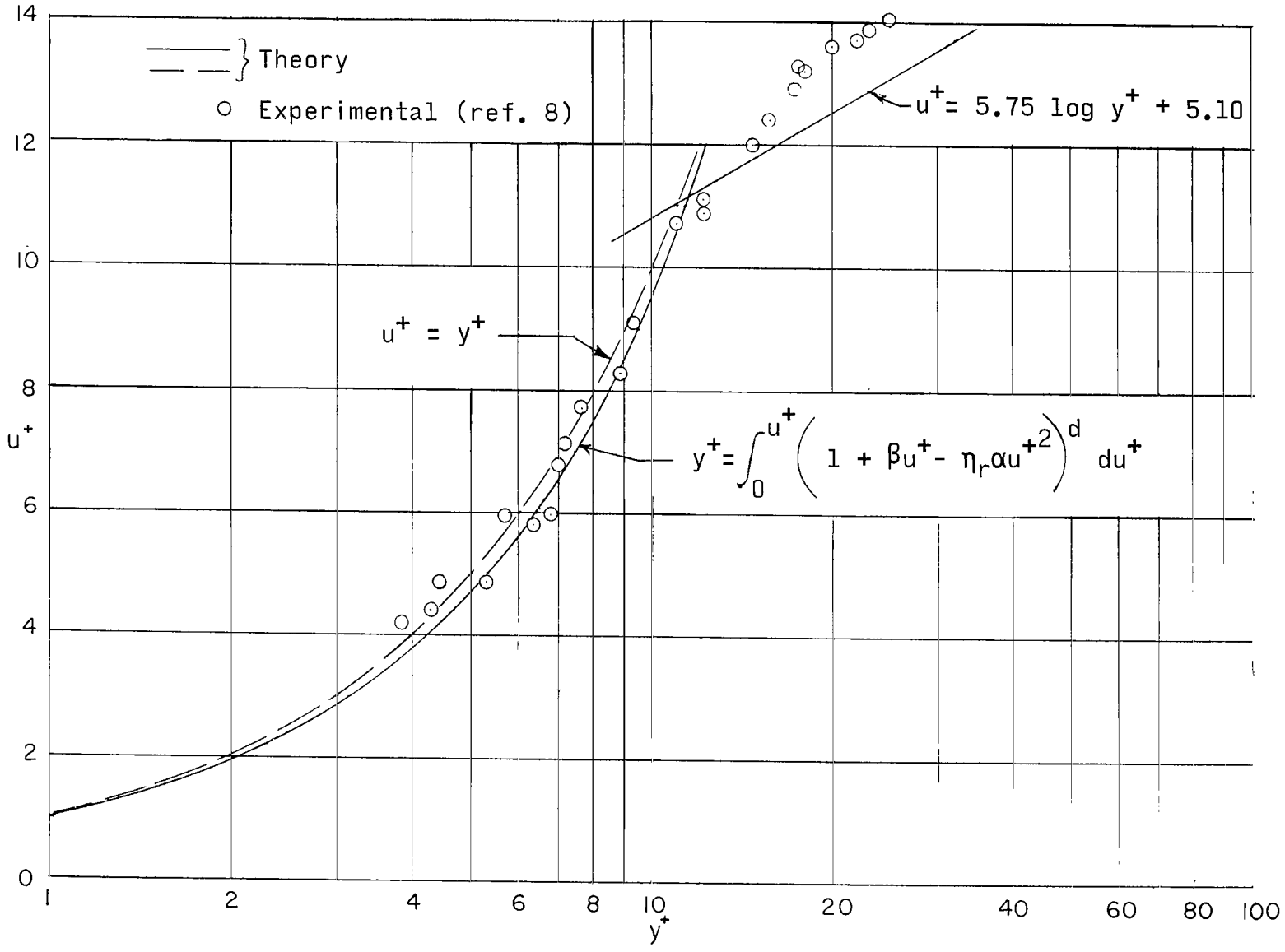

Figure 6.- Comparison of theoretical and experimental laminar sublayer nondimensional velocity profiles. $M_\infty = 9$; $R_{ft} = 1.56 \times 10^6$; $T_w/T_\infty = 7.97$; $C_f = 0.000891$.

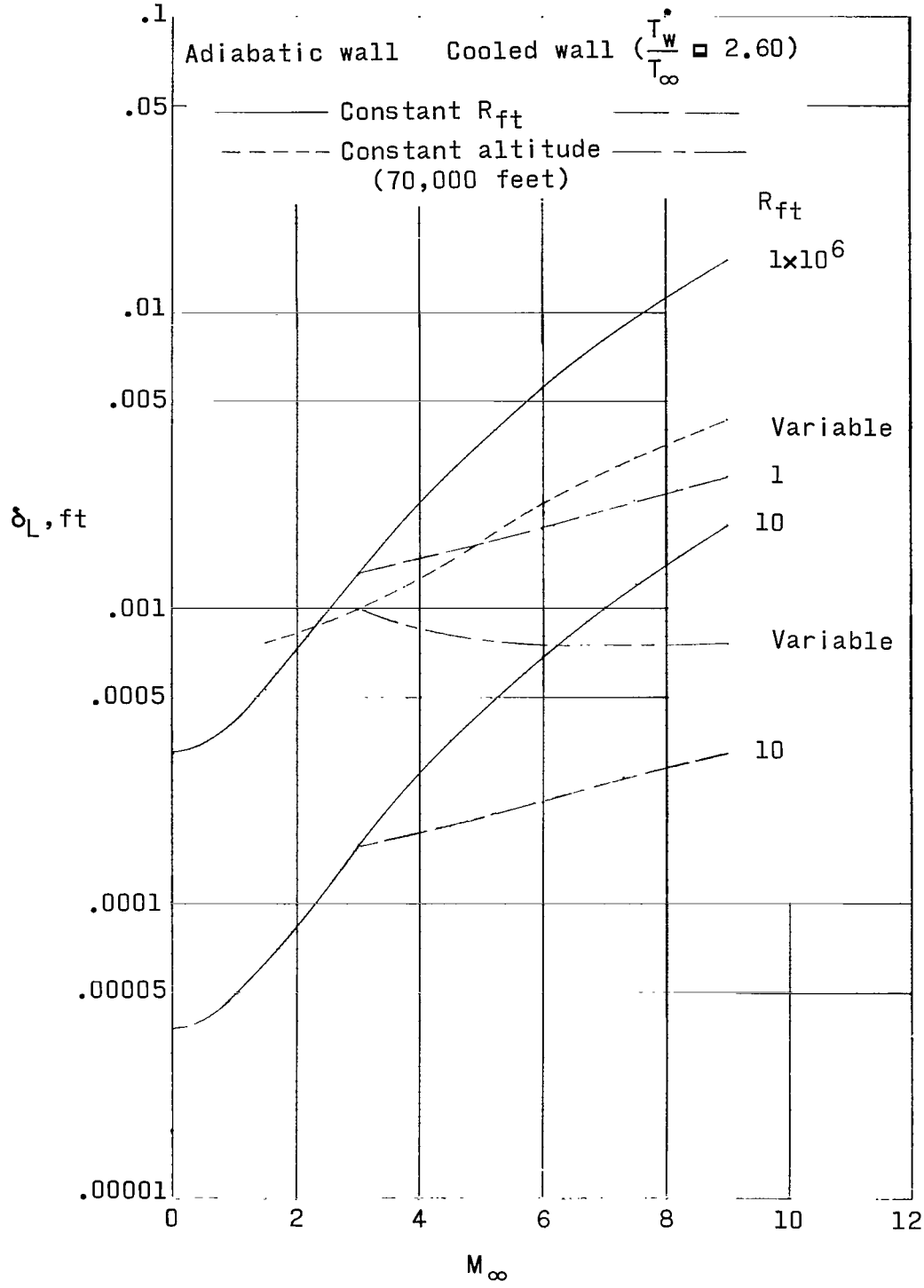

Figure 7.- Variation of δ_L with M_∞. x = 10 feet; T_∞ = 392° R.

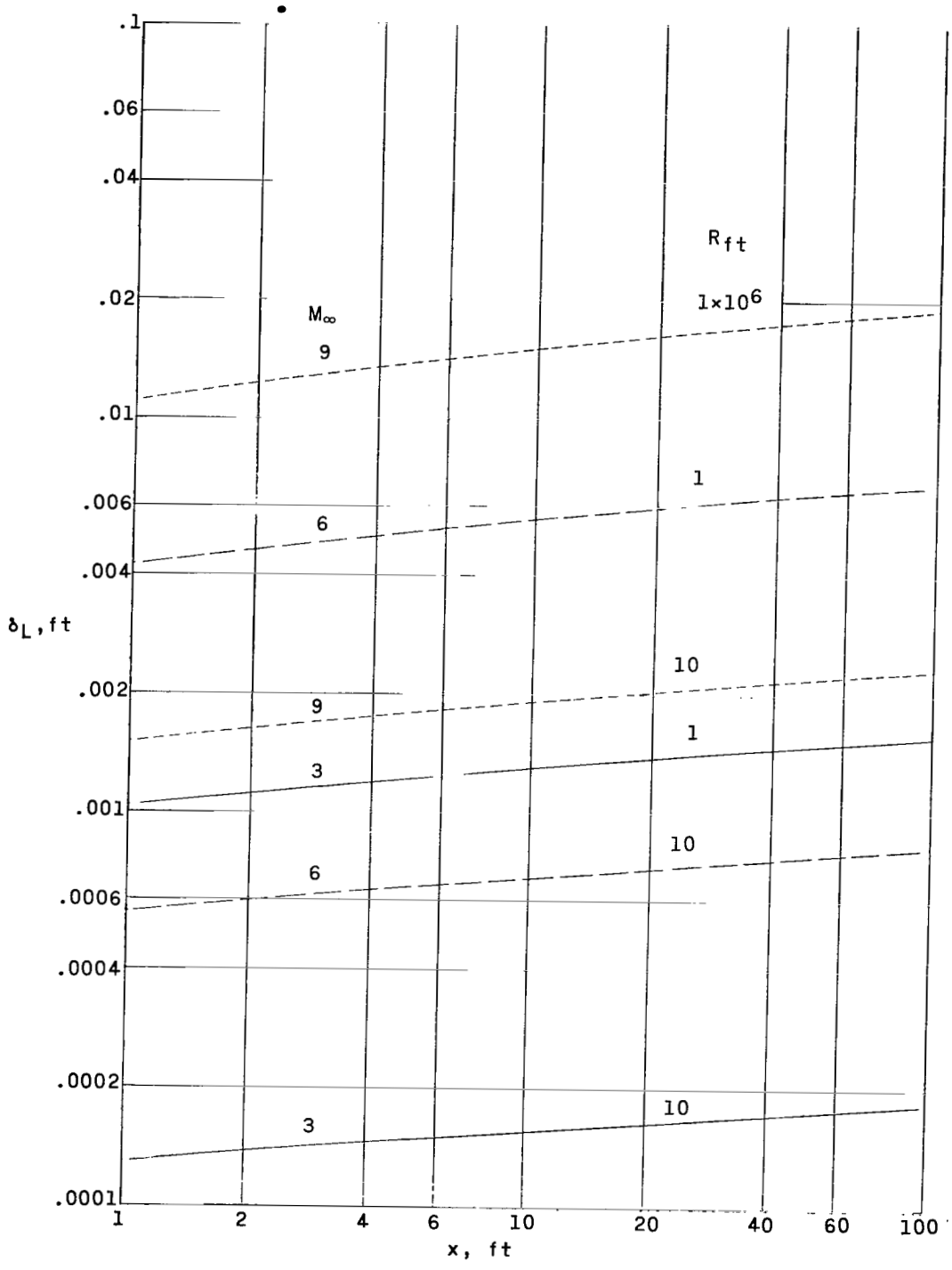

(a) Zero heat transfer.

Figure 8.- Variation of δ_L with x; $T_\infty = 392^\circ$ R.

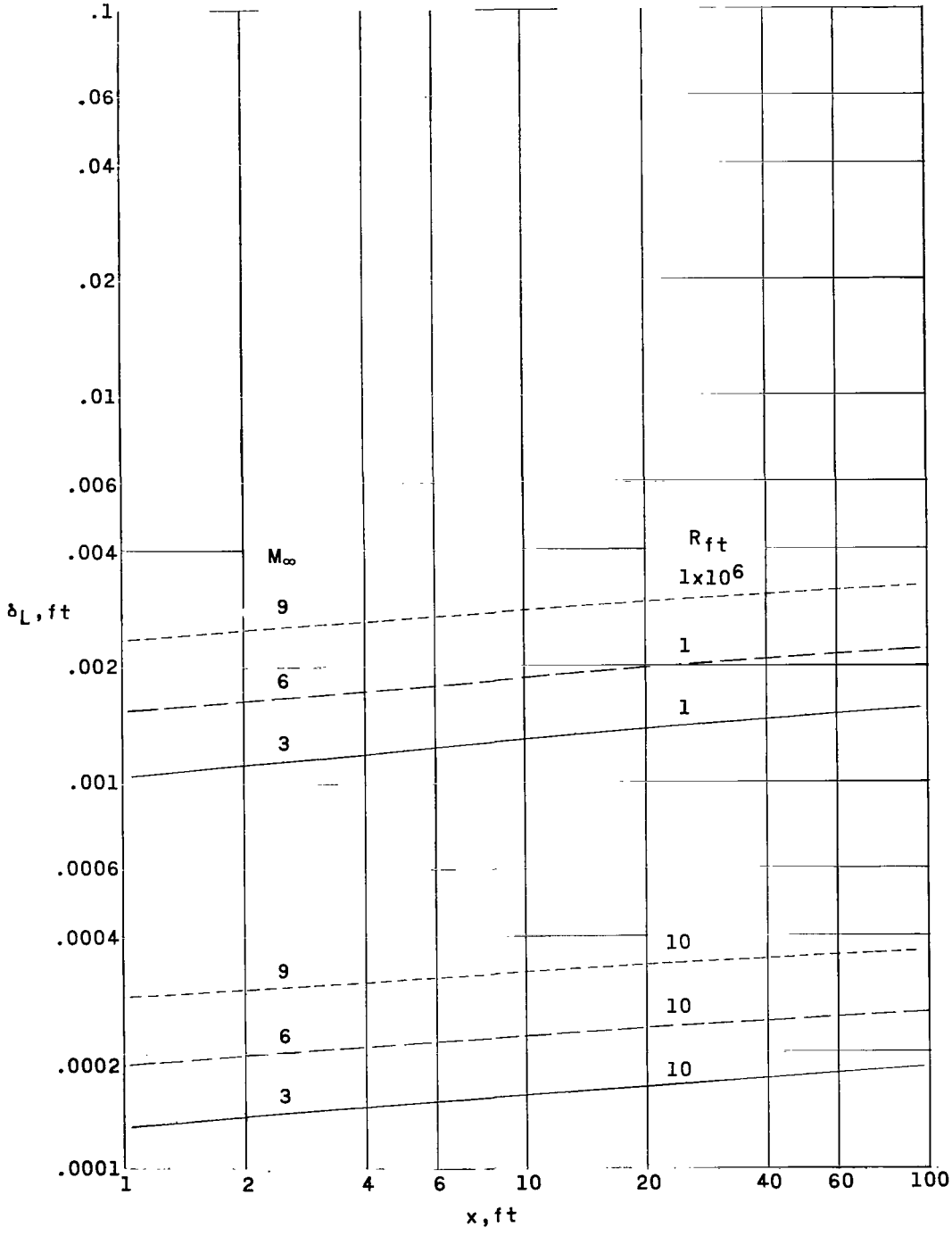

(b) Cooled wall; $T_w/T_\infty = 2.60$.

Figure 8.- Concluded.

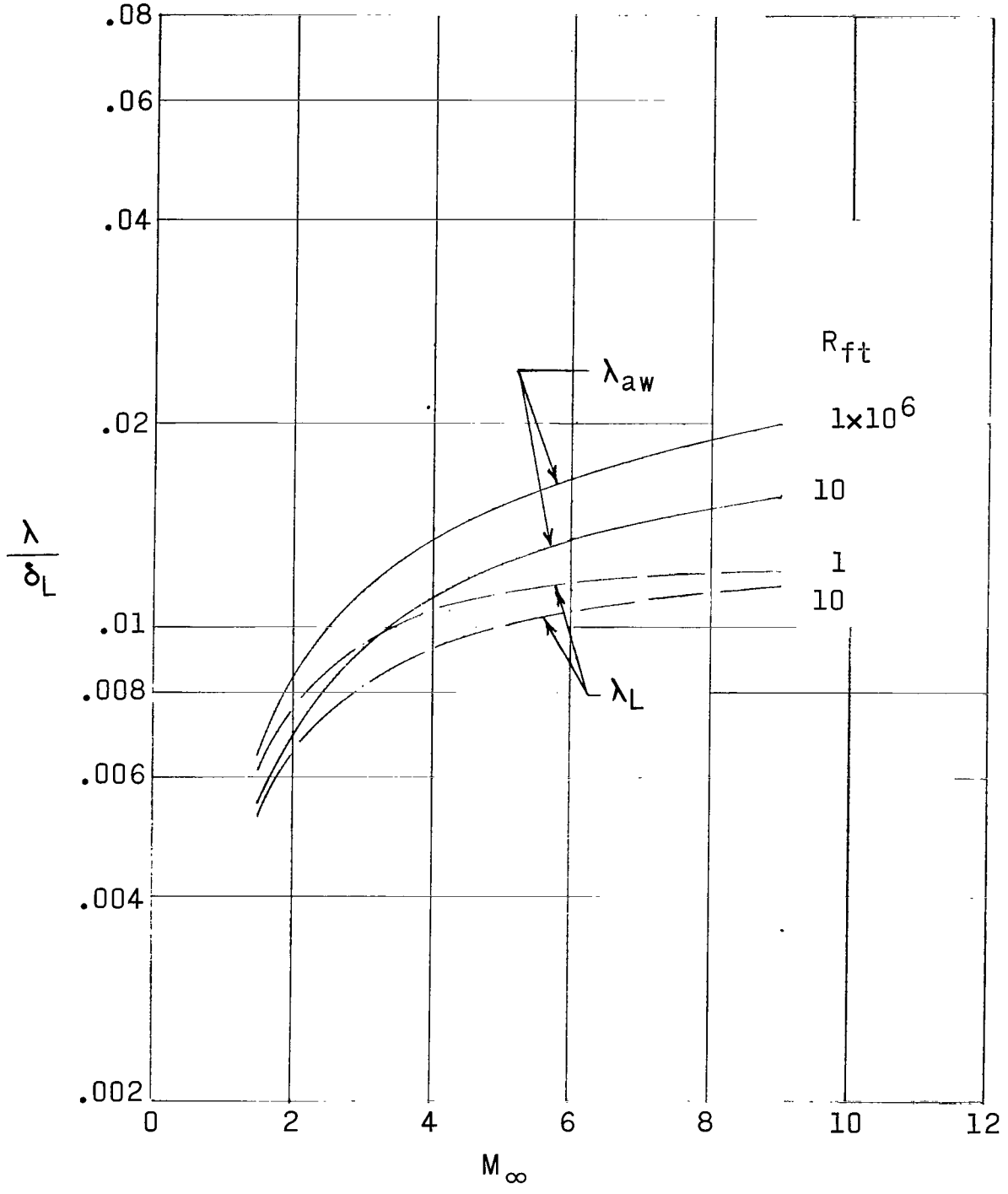

(a) Zero heat transfer.

Figure 9.- Variation of λ/δ_L with M_∞. x = 10 feet; $T_\infty = 392^\circ$ R.

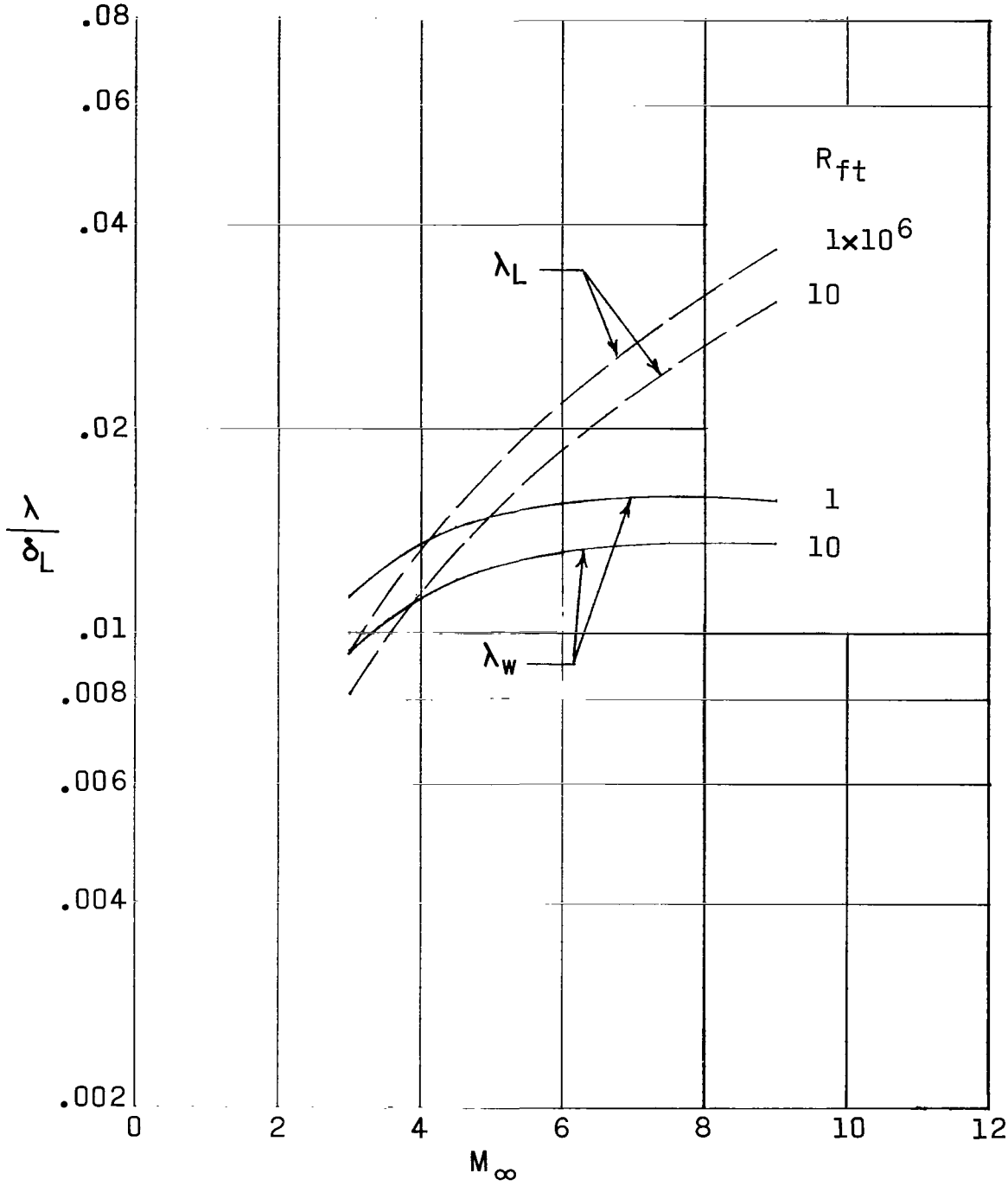

(b) Cooled wall; $T_w/T_\infty = 2.60$.

Figure 9.- Concluded.

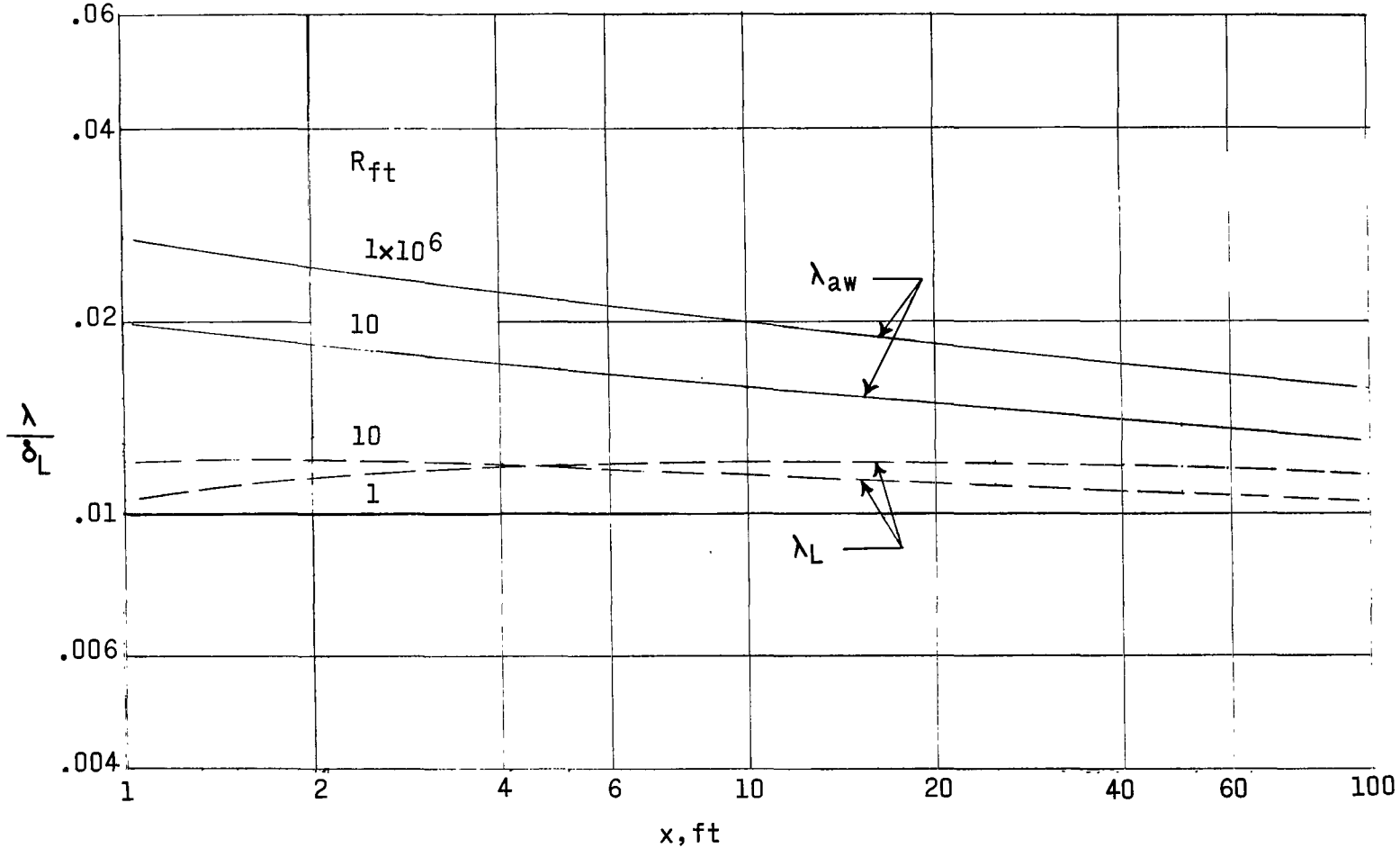

Figure 10.- Variation of λ/δ_L with x at zero heat transfer. $M_\infty = 9$; $T_\infty = 392^\circ$ R.

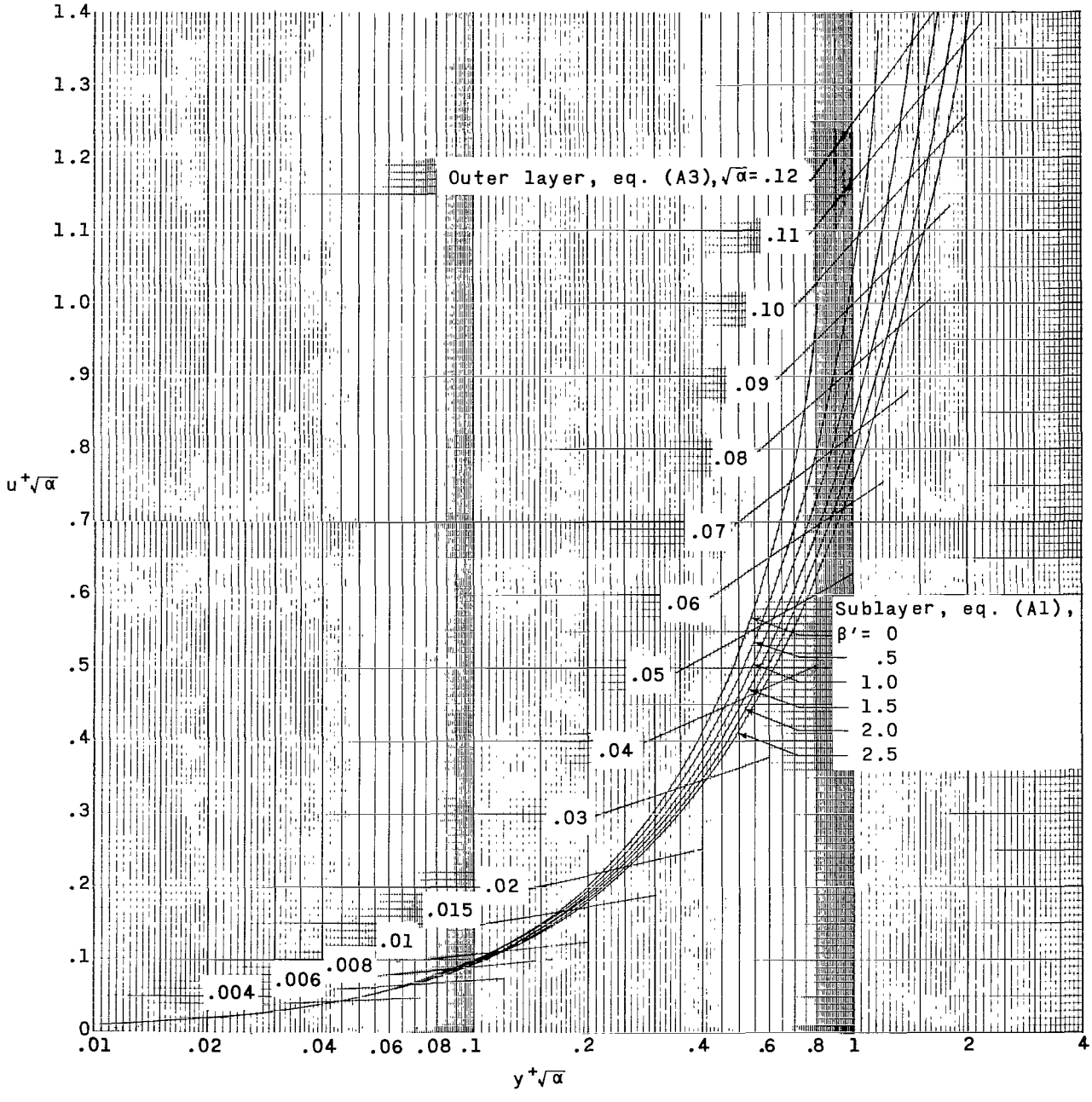

(a) d = 0.5.

Figure 11.- Charts for estimating laminar-sublayer thickness for a constant d.

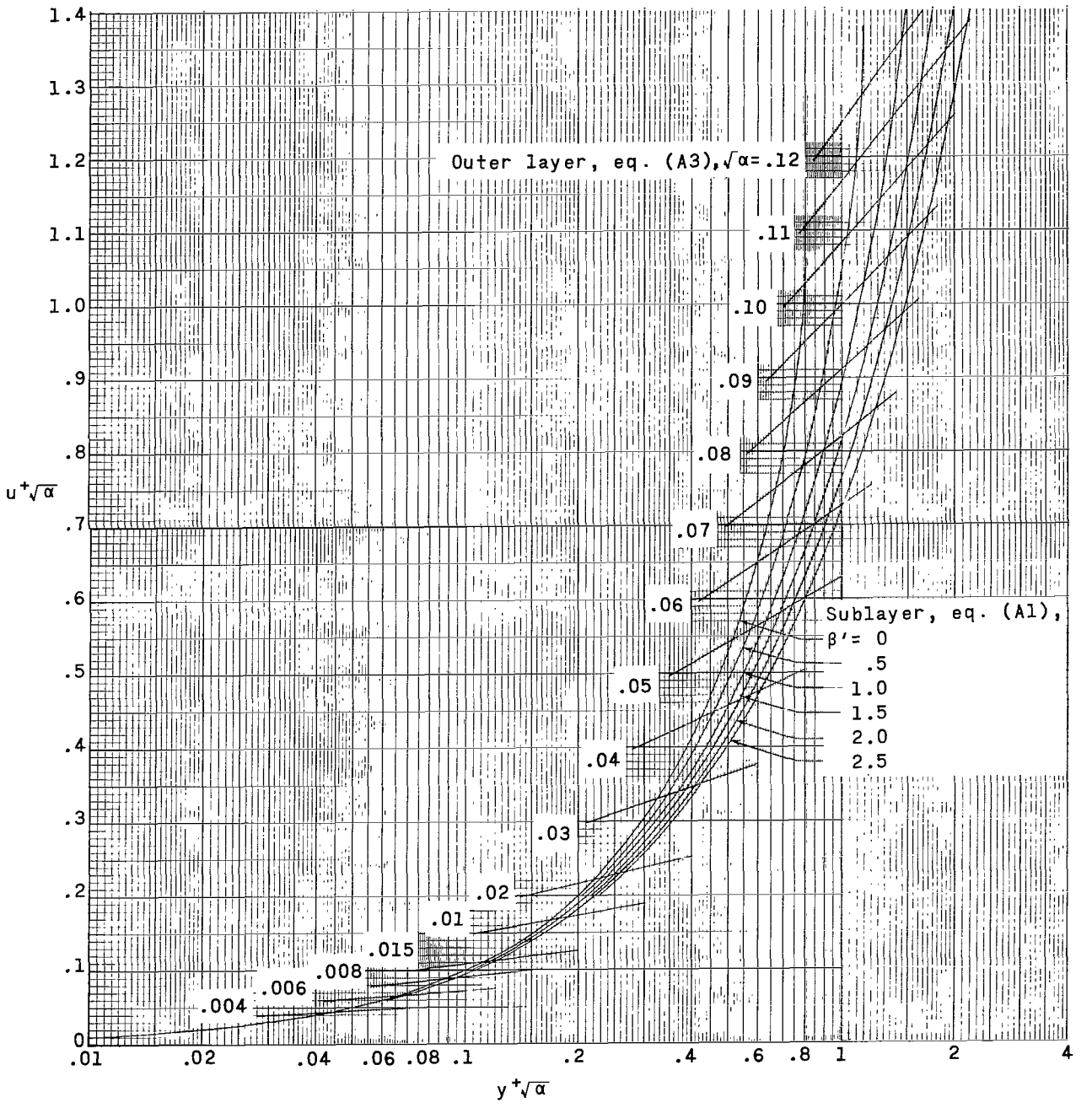

(b) d = 0.6.

Figure 11.- Continued.

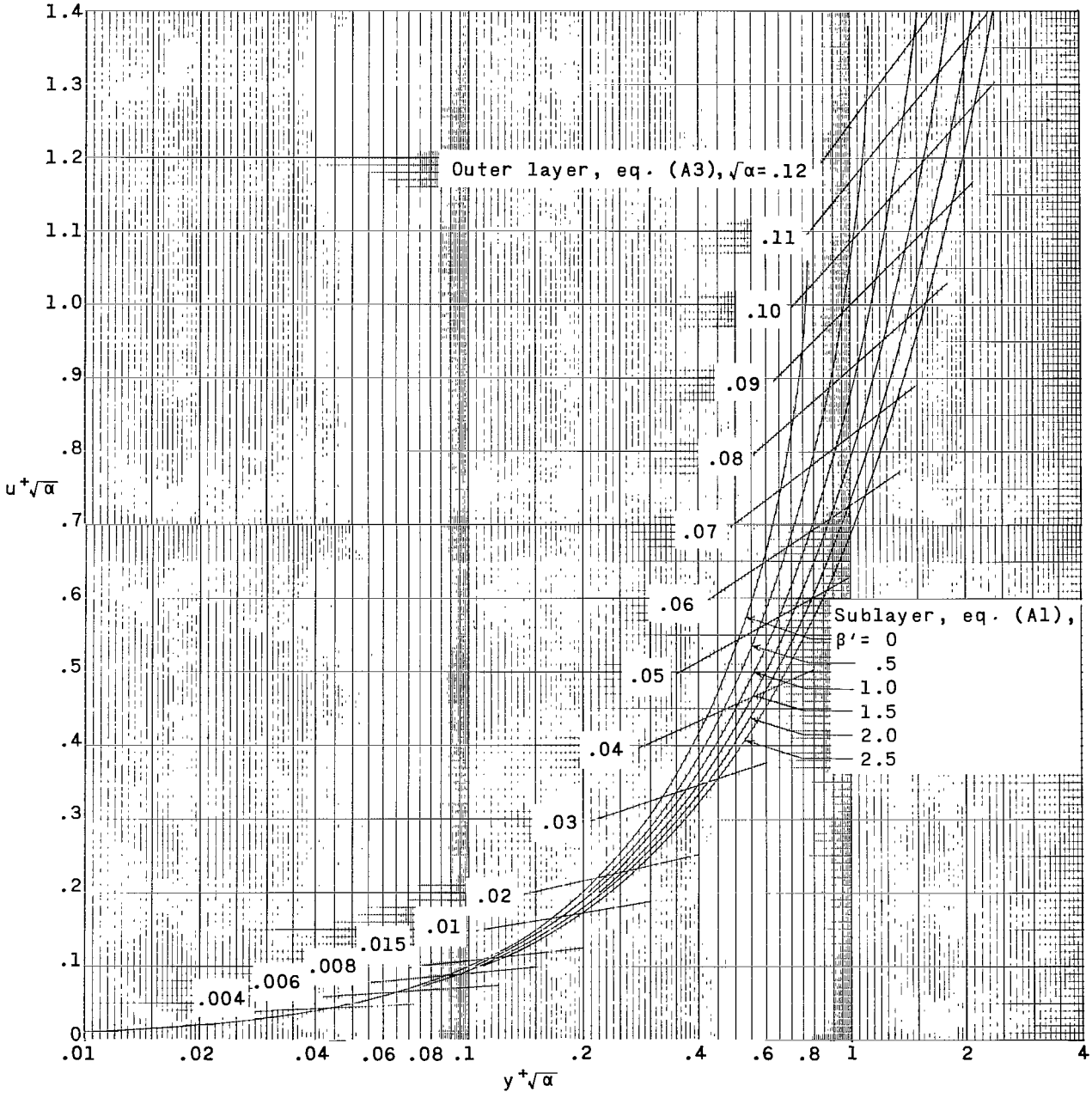

(c) d = 0.7.

Figure 11.- Continued.

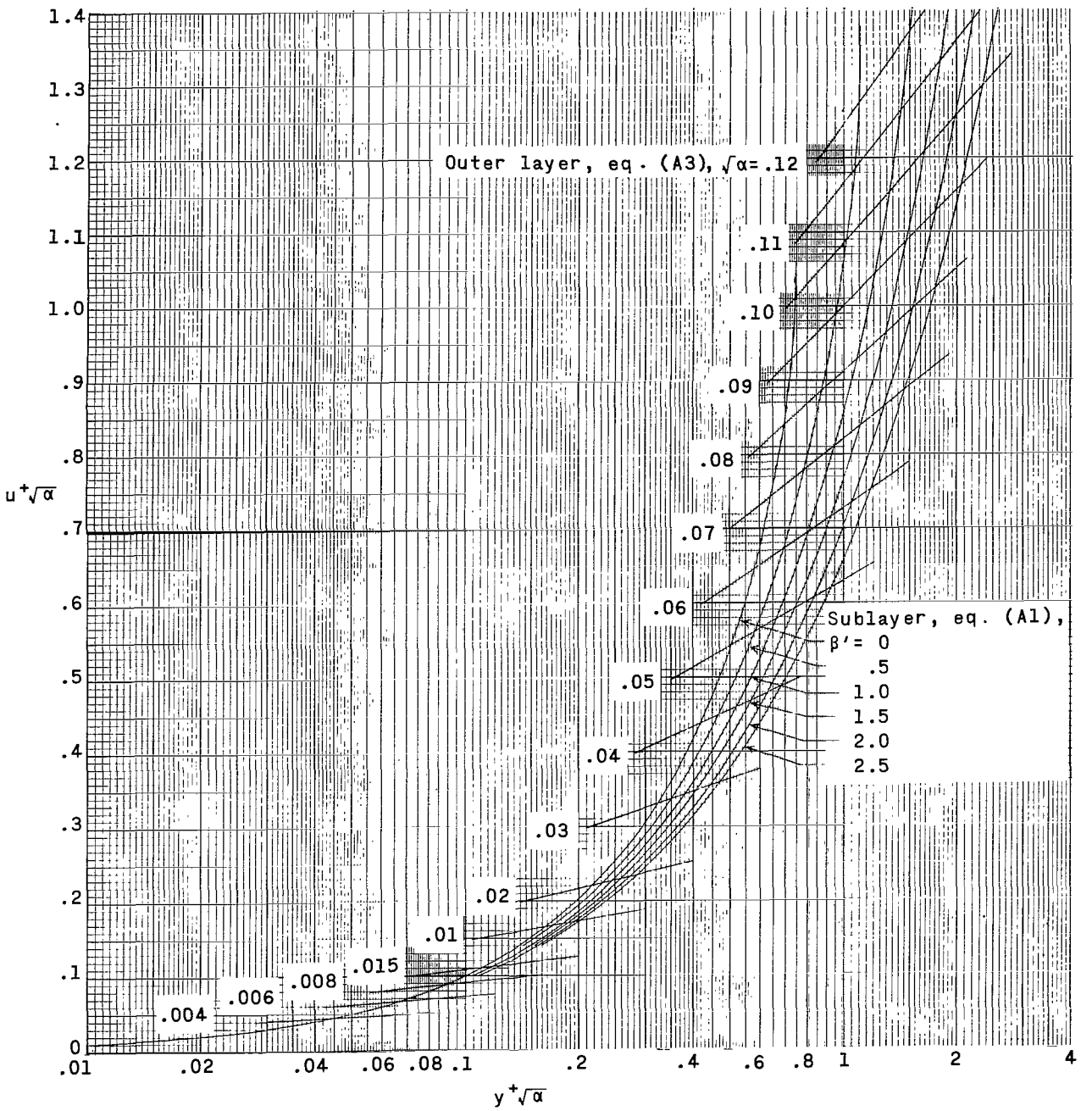

(d) d = 0.8.

Figure 11.- Continued.

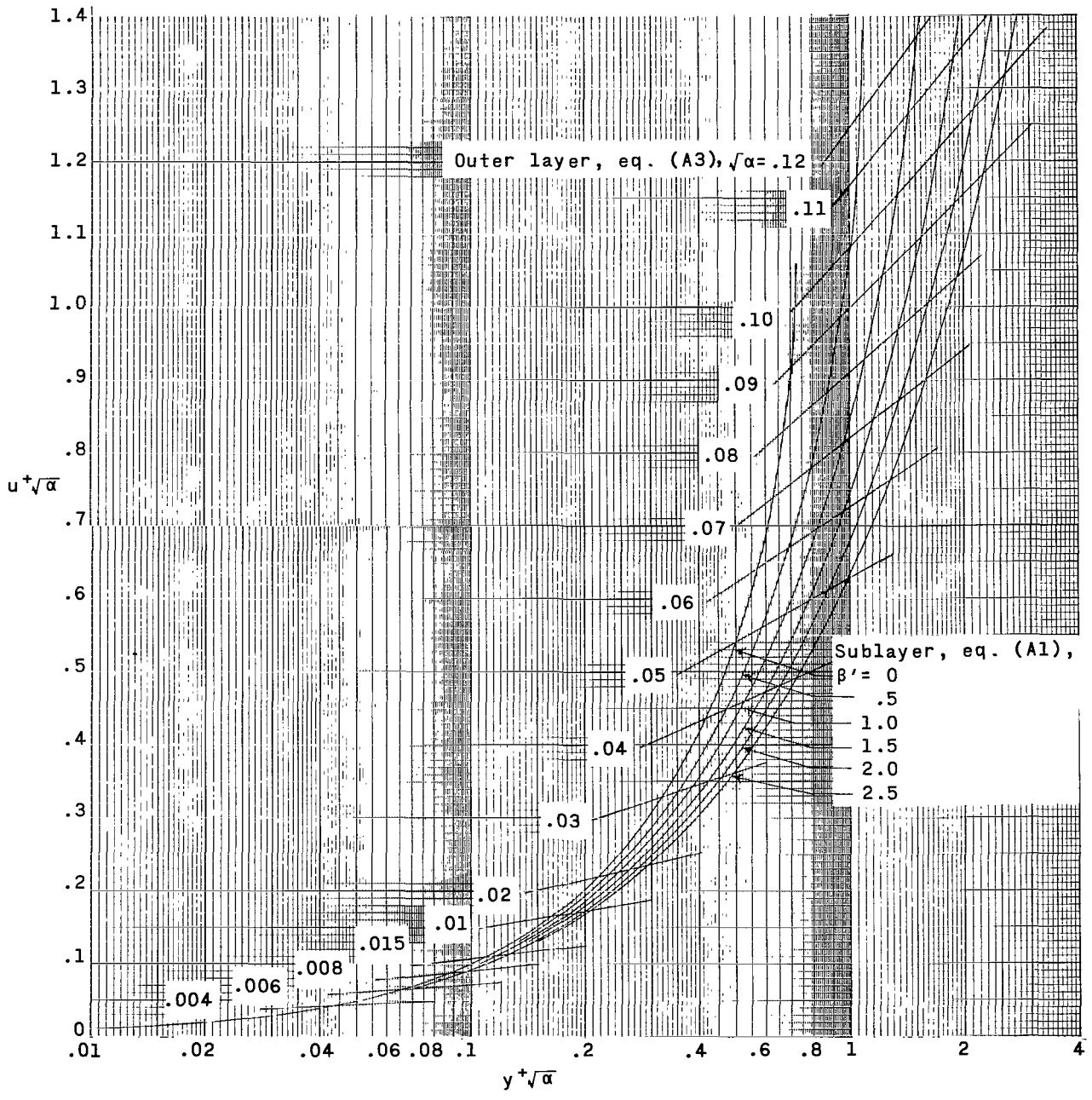

(e) d = 0.9.

Figure 11.- Concluded.

Figure 12.- Variation of viscosity-law exponent d (eq. (A5)) with absolute temperature.

2/5/25
SX

"The aeronautical and space activities of the United States shall be conducted so as to contribute . . . to the expansion of human knowledge of phenomena in the atmosphere and space. The Administration shall provide for the widest practicable and appropriate dissemination of information concerning its activities and the results thereof."

—NATIONAL AERONAUTICS AND SPACE ACT OF 1958

NASA SCIENTIFIC AND TECHNICAL PUBLICATIONS

TECHNICAL REPORTS: Scientific and technical information considered important, complete, and a lasting contribution to existing knowledge.

TECHNICAL NOTES: Information less broad in scope but nevertheless of importance as a contribution to existing knowledge.

TECHNICAL MEMORANDUMS: Information receiving limited distribution because of preliminary data, security classification, or other reasons.

CONTRACTOR REPORTS: Technical information generated in connection with a NASA contract or grant and released under NASA auspices.

TECHNICAL TRANSLATIONS: Information published in a foreign language considered to merit NASA distribution in English.

TECHNICAL REPRINTS: Information derived from NASA activities and initially published in the form of journal articles.

SPECIAL PUBLICATIONS: Information derived from or of value to NASA activities but not necessarily reporting the results of individual NASA-programmed scientific efforts. Publications include conference proceedings, monographs, data compilations, handbooks, sourcebooks, and special bibliographies.

Details on the availability of these publications may be obtained from:

SCIENTIFIC AND TECHNICAL INFORMATION DIVISION

NATIONAL AERONAUTICS AND SPACE ADMINISTRATION

Washington, D.C. 20546